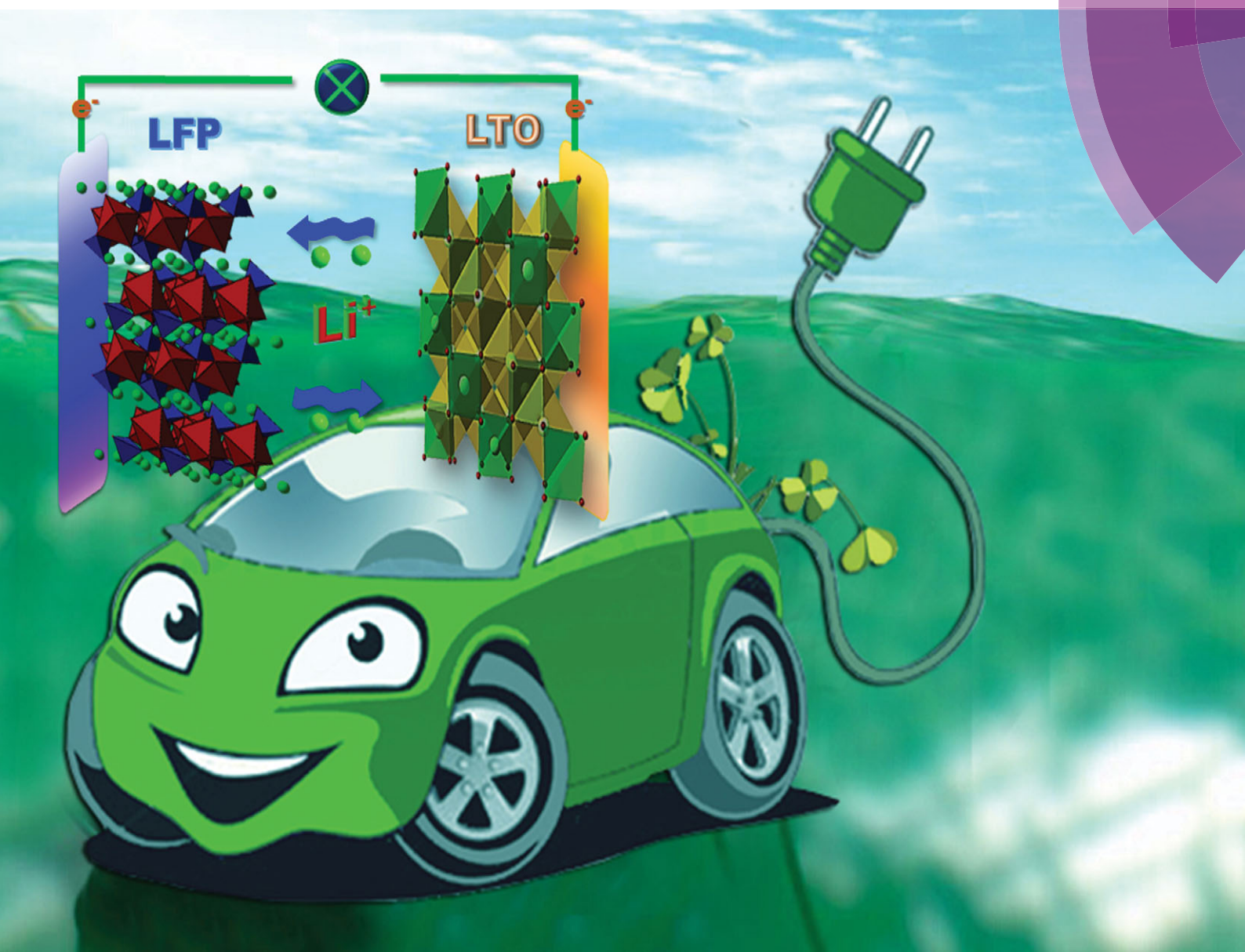


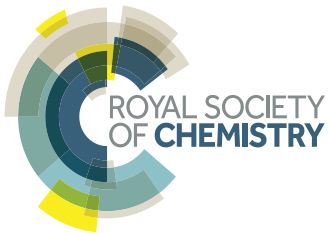
NJC

New Journal of Chemistry
www.rsc.org/njc

A journal for new directions in chemistry



ISSN 1144-0546



PERSPECTIVE

Xiangcheng Sun *et al.*

Advances in spinel $\text{Li}_4\text{Ti}_5\text{O}_{12}$ anode materials for lithium-ion batteries





Cite this: *New J. Chem.*, 2015,
39, 38

Advances in spinel $\text{Li}_4\text{Ti}_5\text{O}_{12}$ anode materials for lithium-ion batteries

Xiangcheng Sun,*^a Pavle V. Radovanovic^b and Bo Cui^a

Anode materials of rechargeable lithium-ion batteries have been developed towards the aim of high power density, long cycle life, and environmental benignity. As a promising anode material for high power density batteries for large scale applications in both electric vehicle and large stationary power supplies, the spinel $\text{Li}_4\text{Ti}_5\text{O}_{12}$ anode has become more attractive for alternative anodes for its relatively high theoretical capacity (175 mA h g^{-1}), stable voltage plateau of 1.5 V vs. Li/Li^+ , better cycling performance, high safety, easy fabrication, and low cost precursors. This perspective first introduces recent studies on the electronic structure and performance, synthesis methods, and strategies for improvement including carbon-coating, ion-doping, surface modifications, nano-structuring and optimization of the particle morphology of the $\text{Li}_4\text{Ti}_5\text{O}_{12}$ anode. Furthermore, practical applications of the commercial spinel lithium-ion batteries are demonstrated. Finally, the future research directions and key developments of the spinel $\text{Li}_4\text{Ti}_5\text{O}_{12}$ anode are pointed out from a scientific and an industrial point of view. In addition, the prospect of the synthesis of graphene– $\text{Li}_4\text{Ti}_5\text{O}_{12}$ hybrid composite anode materials for next-generation lithium-ion batteries is highlighted.

Received (in Montpellier, France)
18th August 2014,
Accepted 3rd October 2014

DOI: 10.1039/c4nj01390e

www.rsc.org/njc

^a Department of Electrical and Computer Engineering and Waterloo Institute for Nanotechnology, University of Waterloo, Waterloo, Ontario, Canada.
E-mail: sunxc824@gmail.com; Tel: +1-519-496-7918

^b Department of Chemistry and Waterloo Institute for Nanotechnology, University of Waterloo, Waterloo, Ontario, Canada



Xiangcheng Sun

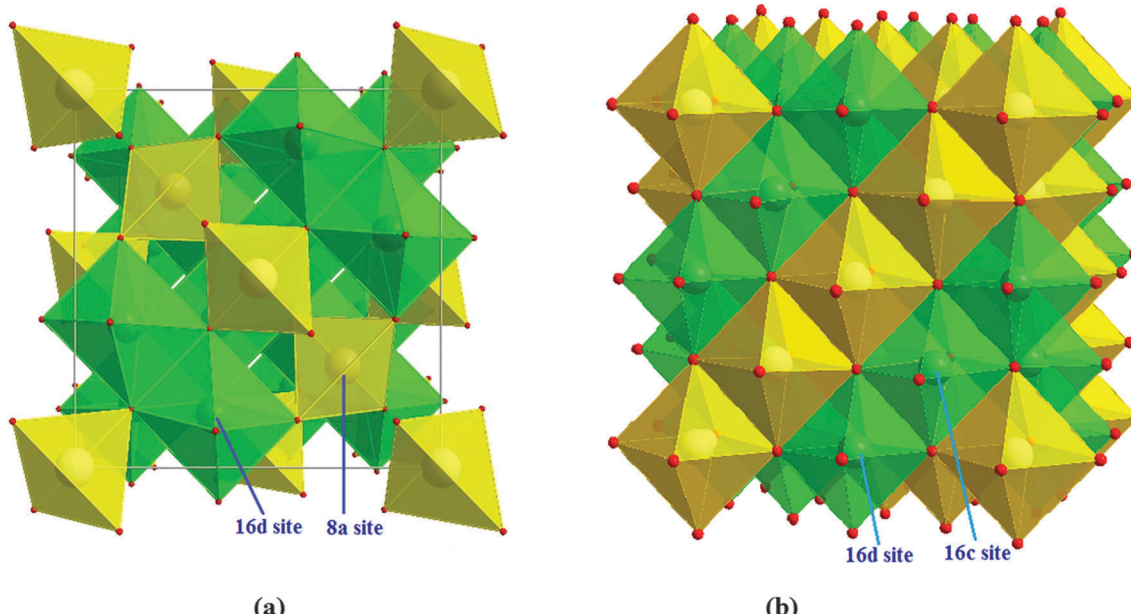
January 2011. His current research interests are focused on the development of nanoscale cathode and anode materials for the design of advanced lithium-ion batteries for high-power backup systems and electric vehicles.

Xiangcheng Sun is currently a PhD researcher in the Nanofabrication Group in the Department of Electrical and Computer Engineering, University of Waterloo, Canada. He received his Master's degree at the Chinese Academy of Sciences in 1997, and his first PhD degree in Materials Science at the University of the State of Mexico in 2000. He has worked as a research scientist for 10 years in the USA, China and Canada before joining the University of Waterloo in



Pavle V. Radovanovic

with nanoscale multifunctionality and his research interests include polymorphism and phase transformations in the nanoscale range, materials for energy, quantum information processing and nanophotonics, and photocatalysis.



Scheme 1 (a) Spinel- and (b) rock-salt-LTO structures. Yellow tetrahedra represent lithium, and green octahedra represent disordered lithium and titanium.

on graphite anode materials can hardly meet the requirements for those high-capacity large-scale applications due to the limitations associated with power density and safety characteristics.^{1,2} In the last decade, much attention has been paid to the search for alternative anode candidates instead of the conventional commercial graphite. Spinel lithium titanate oxide ($\text{Li}_4\text{Ti}_5\text{O}_{12}$, LTO) has been considered the most promising one because of its excellent safety characteristics and long lifetime.^{3–6} Unlike the graphite anode, which expands up to 10 vol% during charging, the LTO anode can accommodate up to three lithium ions per formula unit, which allows a theoretical capacity of 175 mA h g⁻¹ in the spinel structure with negligible volume change during charging and discharging.^{4,7}



Bo Cui

Bo Cui is currently an Assistant Professor in the Department of Electrical and Computer Engineering at the University of Waterloo. He received his Bachelor's degree in physics from Peking University in 1994, and his PhD degree in electrical engineering from Princeton University in 2003. His research is focused on nano- and microstructure fabrication using nanolithography, thin film deposition and etching, as well as bottom-up fabrication techniques. He has published 70 peer-reviewed journal articles and three book chapters, and edited one book. He is the recipient of the 2014 Engineering Research Excellence Award from the University of Waterloo.

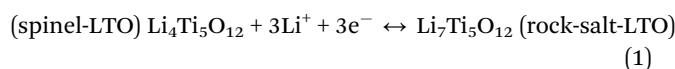
The LTO lattice has a spinel crystal structure with the $F\bar{d}3m$ space group and a cubic symmetry.^{3,8} The lattice constant was calculated to be 0.8364 nm.⁹ Lithium ions occupy the tetrahedral 8a sites and 1/6 of the octahedral 16d sites, while the rest of the octahedral 16d sites are occupied by tetravalent Ti^{4+} ions, and the ratio of lithium ions to titanium ions is 1:5. The oxygen ions are located at the 32e sites. Thus, the spinel-LTO could be expressed as $\text{Li}_{(8a)}[\text{Li}_{1/3}\text{Ti}_{5/3}]_{(16d)}\text{O}_{4(32e)}$ in space notation,^{10,11} where the octahedral 16c sites and the tetrahedral 8b and 48f sites are empty, which is suitable for lithium insertion and extraction.^{12,13} The crystal units of spinel-LTO and rock-salt-LTO are shown in Scheme 1(a) and (b), respectively.

$[\text{TiO}_6]$ is the main frame for the lithium insertion/extraction. Basically, the Li^+ ions occupy the 8a sites forming the spinel structure at the initial stage of discharge. As the lithium ion insertion (discharge) proceeds, three lithium atoms from the 8a sites transfer to 16c sites, and the inserted three lithium ions move to the 16c sites *via* 8a sites. During extraction (charging), the lithium ions are extracted out from the 16c sites *via* 8a sites, and the other lithium atoms move back to 8a sites from 16c sites.¹² Simultaneously, there is the redox reaction of $\text{Ti}^{4+}/\text{Ti}^{3+}$ within the octahedrally coordinated framework, allowing a topotactic transition from the spinel structure of $\text{Li}_4\text{Ti}_5\text{O}_{12}$ (spinel-LTO) to the rock-salt structure of $\text{Li}_7\text{Ti}_5\text{O}_{12}$ (rock-salt-LTO); in space notation: from $\text{Li}_{(8a)}[\text{Li}_{1/3}\text{Ti}_{5/3}]_{(16d)}\text{O}_{4(32e)}$ to $\text{Li}_{2(16c)}[\text{Li}_{1/3}\text{Ti}_{5/3}]_{(16d)}\text{O}_{4(32e)}$.^{11,14,15}

Twenty years ago, Ohzuku and co-authors³ reported that the charge-discharge curve for the LTO electrode as the anode is characterized by a flat and extended voltage plateau at around 1.55 V, which is typical of the phase transition between a Li-rich phase (rock-salt-LTO) and a Li-poor phase (spinel-LTO). Although substantial chemical changes occur during the conversion between the two phases, the corresponding volume change is only 0.2–0.3%. This volume change is associated with the

reduction of the lattice constant from 0.8364 nm to 0.8353 nm during the discharge process. Owing to the negligible volume change, this type of materials is referred to as zero-strain insertion materials, indicating their exceptional reversibility performance as anode materials for LIBs.^{6,16}

Three Ti^{4+} ions are reduced to Ti^{3+} ions during the two-phase transition from spinel-LTO to rock-salt-LTO.^{3,4,6,12} The corresponding electrochemical reaction can be described as:



According to eqn (1), it is obvious that a typical electrochemical reaction between spinel-LTO and rock-salt-LTO takes place during the lithium insertion and extraction processes.

The core–shell model describes a plausible two-phase transition process,^{17–21} as illustrated in Fig. 1. As the lithium intercalation (discharge) proceeds, the spinel-LTO on the surface of the particle is reduced and transformed to rock-salt-LTO. The shell with the rock-salt structure formed in the process becomes thicker with an increasing depth of lithium insertion. Simultaneously, the core with the spinel structure shrinks. At the end of the discharging process, the entire particle becomes rock-salt-LTO. Conversely, the particle transforms from the rock-salt into the spinel phase during the charging (lithium extraction) process. The two types of LTO crystallographic data are summarized in Table 1.²²

As reported earlier, such a spinel-LTO structure provides a very flat voltage plateau of 1.55 V vs. Li^+/Li due to the stable $\text{Ti}^{4+}/\text{Ti}^{3+}$ redox couple during the discharge–charge cycling. During the lithium insertion and extraction processes, a solid electrolyte interface (SEI) film is often formed at a potential below 0.8 V versus Li^+/Li , which consumes active lithium and results in a decrease in specific capacity. However, the potential of LTO is significantly above the reduction potential of most organic electrolytes. Thus, the formation of an SEI film can be avoided on the particle surface by applying spinel-LTO as the anode in the electrochemical battery cell. It has also been demonstrated

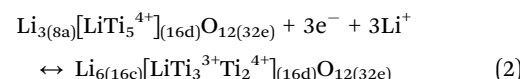
Table 1 Crystallographic data for spinel-LTO and rock-salt-LTO

Anode materials	Wyckoff sites	Atoms	Occupancy	Cell parameters		
				x	y	z
Spinel-LTO	8a	Li1	1.0	0.125	0.125	0.125
	16d	Li2	0.1667	0.5	0.5	0.5
	16d	Ti	0.8333	0.5	0.5	0.5
	32e	O	1.0	0.2625(1)	0.2625(1)	0.2625(1)
Rock-salt-LTO	8a	Li1	1.0	0	0	0
	16d	Li2	0.1667	0.5	0.5	0.5
	16d	Ti	0.8333	0.5	0.5	0.5
	32e	O	1.0	0.2576(3)	0.2576(3)	0.2576(3)

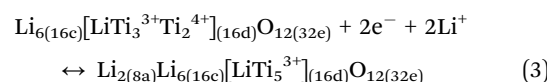
that spinel-LTO shows better thermal stability performance than conventional graphite even below 230 °C.²³

Many investigations already reported that the spinel-LTO anode can accommodate up to three lithium ions per formula unit at a potential of 1.55 V.^{3,4,9,24–28} The insertion mechanism is based on the spinel–rock-salt phase transition, allowing the reduction of 3 Ti^{4+} atoms out of 5, which provides a theoretical capacity of 175 mA h g⁻¹ in the spinel structure.^{11,16,17,29–40}

As stated previously, the lattice parameters remain almost unchanged during lithium insertion and extraction.⁴¹ However, some researchers^{12,42} stated that spinel-LTO can deliver a theoretical capacity of 293–296 mA h g⁻¹ based on the reduction of all Ti^{4+} in the compound with the discharge voltage extended to approximately 0 V. In the literature,^{42,43} it is reported that spinel-LTO exhibited excellent electrochemical performance at different discharge voltage ranges, especially when extended to 0 V. The Li-ion insertion can occur at three crystallographic sites, *i.e.*, the (8a), (16c), and (48f) sites, indicating that the Li ions can intercalate into LTO at a low potential (<1.0 V vs. Li/Li^+). This low-potential intercalation process would lead to an improvement in the energy density of spinel LTO electrodes related to the numbers of octahedral (16c) and tetrahedral (8a) sites and their occupancies between 2.5 and 0.01 V vs. Li/Li^+ . Generally, additional Li^+ ions are inserted into the lattice and located at the octahedral sites in the intercalation process. Meanwhile, the lithium ions initially located at the tetrahedral sites also migrate to the octahedral sites. The intercalation–de-intercalation process can thus be expressed as:



The above reversible reaction takes place in the voltage range of 2.5–1.0 V vs. Li/Li^+ , and 3 mol Li ions are capable of inserting into the octahedral (16c) sites of the LTO lattices, forming a rock-salt structure. In the voltage range of 1.0–0.01 V vs. Li/Li^+ , the other 2 mol of Li ions could be intercalated into rock-salt-LTO, as there are still interstitial sites available in the rock-salt-LTO. The insertion/de-insertion at a low potential can be illustrated as:



Here, vacant tetrahedral (8c) sites are available to accommodate lithium ions under 1.0 V vs. Li/Li^+ , thus enhancing the

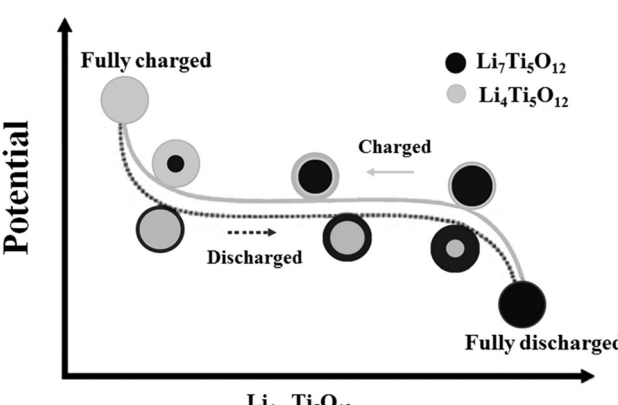


Fig. 1 Illustration of phase transformation from spinel-LTO ($\text{Li}_4\text{Ti}_5\text{O}_{12}$) and rock-salt-LTO ($\text{Li}_7\text{Ti}_5\text{O}_{12}$) during the charging–discharging process. Reproduced with permission from ref. 19. Copyright 2007 Elsevier.

reversible capacity at a low potential. Accordingly, the second stage of the charging plateau contributes to a significant portion of the total capacity of the LTO anodes. Due to this mechanism, LTO can display a reversible capacity of $215.1 \text{ mA h g}^{-1}$ within $2.5\text{--}0.01 \text{ V vs. Li/Li}^+$ at 0.2 C , which is much higher than the conventional theoretical capacity of 175 mA h g^{-1} .

It should be noted that the existence of available free octahedral sites in the lattice of spinel-LTO makes it a good lithium-ion conductor.⁴⁴ However, since the oxidation state of Ti in spinel-LTO is +4, the highest possible valence for Ti, spinel-LTO is a very poor electronic conductor.¹⁹ On the contrary, rock-salt-LTO is a good electronic conductor,¹⁷ which is attributed to the average oxidation state of Ti which is +3.4. This oxidation state suggests the coexistence of Ti^{3+} (60%) and Ti^{4+} (40%) in the lattice, and that rock-salt-LTO is a very poor lithium-ion conductor due to the full occupancy of the (16c) octahedral sites by Li^+ .³⁷ More details about the physical and chemical properties of spinel-LTO are summarized in Table 2.

Applied as an anode, spinel LTO can be coupled to high voltage cathodes such as LiCoO_2 , LiNiO_2 , LiMn_2O_4 , or LiFePO_4 , to fabricate lithium-ion batteries. When compared with its counterparts as anode materials, spinel-LTO is cheaper and easier to prepare than alloy-based anodes, and has better electrochemical properties and better safety than carbonaceous anodes in lithium-ion batteries.⁵³ The comparison between spinel-LTO and other anode materials is summarized in Table 3.

Spinel-LTO has many advantages such as an excellent lithium ion insertion and extraction reversibility, negligible volume or structural change during the charge-discharge process, and a flat potential plateau. However, due to its poor electrical conductivity, spinel-LTO is a very poor electronic conductor, which results in a low specific capacity and poor capability for high rate performance. The practical specific capacity is about $150\text{--}160 \text{ mA h g}^{-1}$, which is much lower than those of other anode materials such as graphite (350 mA h g^{-1}). Therefore, spinel-LTO might not be suitable for high current applications in its native form. Several effective ways have been proposed and explored to improve the conductivity, and one of the most common strategies is to synthesize nanostructured LTO materials, which will be highlighted in detail in the following section. Other attractive ways are to dope the material with metal or non-metal ions in the Li, Ti or O sites, or to introduce surface modifications

via surface coating using conductive species to enhance the surface electrical conductivity.^{62,63}

2. Synthesis methods

The charge-discharge capacity and cycle performance of spinel-LTO are greatly affected by the synthesis method and conditions. The most conventional synthesis methods include solid-state synthesis, hydrothermal method, solvothermal method, sol-gel synthesis, solution-combustion methods, spray pyrolysis, etc.

2.1 Solid-state method

The solid-state reaction method is normally conducted by mixing solid materials and annealing the mixture at high temperatures. This synthetic method is used for the synthesis of spinel anode materials because it is simple and easy. LTO powders are synthesized by a solid-state reaction of lithium and titanium salts at $700\text{--}1000 \text{ }^\circ\text{C}$.^{12,23,26,37,64\text{--}73} The solid precursor materials are ground before their calcination in a furnace. Generally, TiO_2 anatase or rutile is used as the titanium source, and Li_2CO_3 or LiOH as the lithium salt. Solvent (*i.e.* ethanol) is also used as a dispersant to provide a better environment to homogeneously mix the starting materials.

Usually, stoichiometric amounts of TiO_2 and $\text{LiOH}\cdot\text{H}_2\text{O}$ are first dispersed in *n*-hexane to assure homogeneity. The mixture is subsequently heated at $800 \text{ }^\circ\text{C}$ for 24 h in oxygen, after removing the solvent.²⁹ It has been reported that the electrochemical performance is influenced by different synthetic parameters, such as the starting materials (*e.g.*, lithium salt), the calcination temperature, and the calcination time.^{38,74\text{--}76} Hong and co-workers⁷⁷ studied the influence of the starting materials and the annealing temperature on the rate performance and the capacity retention of LTO prepared under different conditions. They used Li_2CO_3 and TiO_2 (either anatase or rutile), which were mixed with de-ionized water after adding 2 wt% of the ammonium salt of polycarboxylic acid as a dispersant. The powder mixtures were exposed to high energy milling for 3 h, and the dried powders were finally calcined at 700 , 800 , or $900 \text{ }^\circ\text{C}$ for 3 h in air. The rate performance and capacity retention were found to have different values. Yao and co-workers³⁷ have reported that LTO prepared using a solid-state reaction can be

Table 2 Summary of physical and chemical properties of spinel-LTO as an anode for LIBs

Advantages	<ul style="list-style-type: none"> • Cheap, safe, and easy to prepare^{3,4,6,45} • Good lithium-ion mobility, environmentally friendly⁴⁶ • Higher lithium-ion mobility than graphite⁴⁷ • Zero-strain insertion that provides little volume variation and negligible lattice parameter changes during charge-discharge process^{3,48} • Almost free of solid electrolyte interphase (SEI) film, little gas evolution and little electrolyte decomposition¹² • Good Li-ion insertion/extraction reversibility and good structural stability³⁴ • Stable performance at high temperatures (higher than $60 \text{ }^\circ\text{C}$), high-rate discharge performance even at 10 C⁴⁹ • High columbic efficiency (> 95% at 1 C) and thermodynamically flat discharge profile at 1.55 V (<i>vs.</i> Li/Li^+)⁴⁸
Disadvantages	<ul style="list-style-type: none"> • Low electronic conductivity ($< 10^{-13} \text{ S cm}^{-1}$ at room temperature)⁵⁰ • A cubic closely packed oxygen array, Li-ion diffusion coefficient is generally about $10^{-6} \text{ cm}^2 \text{ s}^{-1}$ (ref. 4 and 7) • A theoretical specific capacity of 175 mA h g^{-1}, a relative practical specific capacity of $150\text{--}160 \text{ mA h g}^{-1}$, compared with graphite ($\sim 300 \text{ mA h g}^{-1}$)^{51,52}

Table 3 Comparison of performance between spinel LTO and other anode materials

Anode materials	Potential (V)	Capacity (mA h g ⁻¹)	Remarks and references
Graphene	0.05	540	<ul style="list-style-type: none"> • Superior electronic conductivity compared to graphitic carbon⁵⁴ • Broad electrochemical window⁵⁴ • High surface area of over 2600 m² g⁻¹ (ref. 54) • Easy coating⁵⁵
Spherical graphitized mesocarbon microbeads	0.05	320–330	
Pitch-based graphite	0.05	350	
Carbon-coated natural graphite	0.05	360–365	
Si(Li _{4.4} Si)	0.5–1	4200	
Sn	0.6	990	
LiC ₆	0.1–0.2	372	
InSb, Cu ₂ Sb	0.9	250–300	
TiO ₂ -B	1.5–2.0	305	
TiO ₂ -AB (acetylene black)	1.5–2.0	320	
Rutile TiO ₂	1.5–2.1	270	<ul style="list-style-type: none"> • Poorer electrochemical properties than anatase TiO₂ (ref. 58) • Low costs, nontoxicity, low volume expansion (3–4%) during lithium insertion⁵⁹ • Environmentally friendly⁵⁹
Anatase TiO ₂	1.5–2.1	336	<ul style="list-style-type: none"> • Excellent capacity retention during cycling⁵⁷ • Severe capacity fading⁵⁸ • Safety issues^{1,23} • Poor cyclability¹ • Good electrochemical reversibility and high rate performance⁶¹ • Higher electric conductivity⁶¹ • Pure LiTi₂O₄ is difficult to synthesize⁶¹ • Good structural stability and safety^{3,4,6} • Better coulombic efficiency > 95% at 1 C⁴⁸ • Flat discharge profile at 1.55 V (vs. Li/Li⁺)⁴⁸ • Stable high-temperature performance even at 60 °C^{49,51} • Good Li-ion insertion/extraction reversibility^{3,4,6} • Free of solid electrolyte interphase (SEI)¹²
Li ₂ Ti ₃ O ₇	1.3–2.1	240	
LiTi ₂ O ₄	1.17–1.75	133.6	
Li ₄ Ti ₅ O ₁₂	1.0–2.0	150–160	

cycled in the voltage range between 0 and 3.0 V with excellent cyclability and a capacity of about 200 mA h g⁻¹. Rutile TiO₂ is more desirable in producing high purity LTO than anatase TiO₂, due to the anatase-to-rutile phase transformation, which is found to be more rigid in the solid-state reaction than the intact rutile phase.^{77–79} The formation mechanism of spinel-LTO, using a solid-state reaction between Li₂CO₃ and TiO₂, for the application in lithium-ion batteries was proposed.⁷⁸ A schematic model was provided to explain the different spinel-LTO formation mechanisms from pure anatase and anatase/rutile mixed TiO₂. According to this model, the anatase/rutile-phase boundaries played an important role in enhancing the solid-state reaction.⁷⁸ The utilization of rutile TiO₂ as a starting phase would be desirable in enhancing the spinel-LTO content, which is the key factor for increasing the specific capacity.⁷⁷ The specific capacity of spinel-LTO prepared from anatase TiO₂ depends significantly on the milling method (*i.e.*, high energy milling, ball milling) and the heat treatment temperature, whereas spinel-LTO prepared from rutile TiO₂ showed a uniform capacity of 160 mA h g⁻¹, regardless of the synthesis parameters, owing to their high LTO phase content. Overall, spinel-LTO powder with a specific capacity of 165 mA h g⁻¹ could be synthesized by optimizing the milling method and the starting materials.⁷⁷ The conventional solid-state method would easily cause aggregation of the LTO particles at the expense of loss of the material's nanostructure. The desired properties of the LTO particles are difficult to realize as the expected morphology would be destroyed through particle aggregation. A modified synthesis of LTO, based on the solid-state method, has also

been developed. Li and co-authors⁸⁰ demonstrated a microwave reaction system for the preparation of LTO particles with less aggregation. The starting materials Li₂CO₃ and anatase TiO₂ were thoroughly mixed in a stoichiometric ratio. Since Li₂CO₃ and TiO₂ could only absorb a small amount of microwaves at relatively low temperatures, the double crucible system was applied to achieve the high temperature needed for the solid-state reaction, with charcoal used as a heating medium between two porcelain crucibles. The microwave reaction system was placed in the centre of a rotating plate of a modified microwave oven, and irradiated at 500–700 W for 10–15 min. A molten-salt reaction^{81,82} was also used as a modified solid-state method by introducing salts such as LiCl, NaCl or KCl into the conventional solid-state reaction. A composite LiCl-KCl can dramatically decrease the melting point, and provide a liquid reaction environment, which can accelerate the diffusion and promote the crystal formation.⁸¹ The spinel-LTO that was obtained using the eutectic molten-salt method, using the mixtures with a molar ratio of LiCl/KCl = 1.5, achieved a high initial discharge capacity of 169 mA h g⁻¹, a high charge-discharge efficiency of 94% at a 0.2 C rate, and also good rate performance from 0.2 to 5 C.⁸¹

2.2 Hydrothermal method

The hydrothermal synthesis is performed in autoclaves at a controlled temperature and/or pressure with the reaction in aqueous solution, followed by a calcination step at temperatures above 500 °C. This method has been widely used for the production of uniform small particles in industry.

Many research efforts have been dedicated to improve the hydrothermal method for pure spinel-LTO anode materials.^{46,83–90} For example, Lai and co-authors⁸⁷ reported a hydrothermal method to prepare LTO; they employed TiOSO_4 and $\text{LiOH}\cdot\text{H}_2\text{O}$ as the starting materials and water as the solvent with a certain amount of urea. After thoroughly mixing the starting materials in water containing urea, the resultant solution was transferred into a Teflon-lined autoclave and treated at 180 °C for 24 h. The precipitate was harvested and then calcined at 500 °C for 2 h under an Ar atmosphere. Chen and co-workers⁴⁶ reported a hydrothermal method to obtain hierarchical layered LTO nanosheets using titanium tetra(isopropoxide) and LiOH as the starting materials. Hydrogen peroxide was used to control the hierarchical morphology of LTO. Typically, 1 ml of 30% hydrogen peroxide was dispersed in 20 ml of 0.4 M LiOH, followed by the addition of 2 mmol titanium tetra(isopropoxide). The solution was transferred into a 30 ml Teflon-lined stainless autoclave and maintained at 130 °C for 12 h. The resulting white precipitate was recovered by centrifugation, thoroughly washed with deionized water, and then dried in an oven at 80 °C. Finally, the as-prepared sample was calcined in a muffle furnace at 550 °C for 6 h in air. Using this method, hierarchical sawtooth-like LTO nanosheets were obtained.

2.3 Solvothermal method

The difference between the solvothermal and the hydrothermal methods is the solvent used in the preparation process. The solvothermal method uses a non-aqueous solution, *e.g.*, ethanol, while the hydrothermal method employs water as the solvent. Since a variety of organic solvents with high boiling points can be selected in the solvothermal method, the temperature can be much higher than that in the hydrothermal method. Besides, the solvothermal method is characterized by better control of the size and shape distributions and a better crystallinity of the LTO nanoparticles relative to the hydrothermal method. The solvothermal method has been an alternative method to prepare LTO with small and uniform particles.^{60,91–93} For example, lithium hydroxide (LiOH), tetrabutyl titanate and ethanol were used as the starting materials. The reaction system was formed using 0.1 mol tetrabutyl titanate dissolved in 100 ml ethanol, followed by the addition of 0.1 or 0.08 mol LiOH. The undissolved LiOH particles were suspended in the orange-like solution. The alcoholic suspension was solvothermally treated at 140 °C for 24 h in a 150 ml autoclave under autogenous pressure. The pressure generated in the autoclave at 140 °C is ~747 kPa. After the solvothermal reaction, the produced powders were washed and filtered with ethanol and then deionized water (five times) to eliminate the unreacted reagents, followed by drying at 80 °C for 24 h in air.⁶⁰

2.4 Sol-gel method

The sol-gel method is a wet-chemical technique widely used in materials science and ceramic engineering. The synthesis of LTO particles using the sol-gel method results in particles with a nearly cubic morphology and a narrow size distribution, which also exhibit a high initial discharge capacity and good

cycling performance.⁹⁴ Unfortunately, the reaction materials usually include organic acids such as citric acid, which have a high cost, so this method is unsuitable for large-scale applications.

A colloidal suspension (sol) acts as the precursor for an integrated network (gel) of either discrete particles or network polymers. Typical precursors are metal alkoxides, metal salts (such as chlorides and acetates), and organic metal compounds which undergo various forms of hydrolysis and polycondensation reactions.^{51,95–99} The sol-gel method can avoid the problem caused by the solid-state method.¹⁰⁰ It is an environmentally friendly process as it uses an aqueous solution. This process can easily control the phase structure, composition homogeneity, crystallite size, monodispersity and microstructure.¹⁰¹ It also has the advantage of low fabrication costs, relatively easy stoichiometry control, high deposition rate, low synthesis temperature, shorter heating time, and better crystallinity.^{102,103}

It is a desirable method to obtain LTO with good homogeneity, uniform morphology, and a narrow size distribution.⁹⁴ However, it is difficult to control the synthesis conditions in terms of the large quantities of solvents and organic materials such as citric acid, ethylene glycol and polyvinyl alcohol needed, which prevents its extensive application in energy storage.⁸¹ Moreover, the sol-gel method also requires a post-synthetic high-temperature calcination at 800 °C or higher temperatures to prepare a pure spinel-LTO phase, which results in an undesirable particle growth.⁸⁴ In order to obtain spinel-LTO with optimal electrochemical performance, much effort has been invested to optimize the sol-gel synthetic approach. Hao and co-authors⁵¹ reported a novel sol-gel method using triethanolamine (TEA) to produce spinel-LTO with an initial discharge capacity of 168 mA h g⁻¹. They also reported that the spinel-LTO synthesized using a Li/Ti atomic ratio 4:5 and a molar ratio of citric acid to total metal ions of $R = 1/2$, exhibited an initial discharge capacity of 167 mA h g⁻¹ at 23.5 mA g⁻¹.¹⁰⁴ The authors further investigated an oxalic acid-assisted sol-gel method to synthesize LTO, which exhibits a capacity of 171 mA h g⁻¹ in the first cycle and of 150 mA h g⁻¹ after 35 cycles under optimal calcination conditions at 800 °C for 20 h.¹⁰⁵

Alias and co-authors⁹⁶ used lithium *tert*-butoxide and titanium isopropoxide as the starting materials, which were mixed together in ethanol, and the residue was harvested and finally sintered at different temperatures (700–1000 °C) and times (1–5 h). Khomane and co-workers⁹⁷ employed hexadecyltrimethylammonium bromide (CTAB) as a cationic surfactant to control the crystal growth of LTO. In a typical process, CTAB was dissolved in 100 ml ethanol under magnetic stirring. Four grams of lithium acetate dihydrate was dissolved in the above solution with continued magnetic stirring. Titanium(IV) isopropoxide was added to the above solution dropwise by keeping the molar ratio Li : Ti = 1 : 1.25. The temperature of the solution was raised to 90 °C and it was stirred continuously to form a gel. The gel was aged at 100 °C for 24 h in air and the precursor was decomposed at 400 °C for 4 h followed by calcination at 800 °C for 12 h in air. The average discharge capacity of the prepared LTO after 20 cycles was ~160 mA h g⁻¹ at a constant current density of 21.37 mA g⁻¹.

2.5 Solution-combustion methods

The solution-combustion method is a facile and economical technique for the preparation of nanomaterials for a variety of applications such as fuel cells and lithium-ion batteries. It also has the advantage of relatively simple infrastructure requirements, the formation of high-purity products with size and shape control, and stabilization of metastable phases.¹⁰⁶ The initial reaction medium is an aqueous or non-aqueous solution, and fuels are used as a C and H source to liberate heat *via* combustion. The complexes formed with the metal ions could facilitate the homogeneous mixing of the cations in solution.^{107,108} Prakash *et al.*¹⁰⁹ reported a solution-combustion synthesis of LTO nanopowders using titanyl nitrate [TiO(NO₃)₂] and LiNO₃ as the oxidant precursors and glycine as the fuel. In a typical preparation, an aqueous redox mixture containing stoichiometric amounts of titanyl nitrate, LiNO₃, and glycine were put into an alumina crucible and placed into a muffle furnace pre-heated at 800 °C. The synthesis of the LTO nanoparticles, crystallizing in a cubic spinel-phase, was completed in less than one minute. TEM images indicate that the primary particles are agglomerated crystallites of varying sizes between 20 and 50 nm with a three-dimensional (3D) interconnected porous network. It was found that the LTO prepared using the combustion technique is superior in terms of both high rate-capability and capacity retention compared with those of the solid-state method, which can be attributed to the high crystallinity and nanosized particles of LTO. Raja and co-authors¹¹⁰ reported a novel aqueous combustion process using the common amino acid alanine as the fuel to synthesize LTO, which showed a uniform morphology with an average particle size in the range 40–80 nm and an optical band gap at 1.8 eV. Yuan and co-workers¹¹¹ reported a glycine-nitrate combustion process for the preparation of spinel-LTO, which showed high electrochemical performance and reached a capacity of 125 mA h g⁻¹ at 10 C with a fairly stable cycling performance. In addition, they⁷⁹ reported a cellulose-assisted combustion process to synthesize pure-phase spinel LTO at reduced temperatures using anatase TiO₂ as the titanium source. Compared with the solid-state reaction, the cellulose-assisted process produced LTO with a smaller particle size and higher specific capacity due to the lower synthesis temperature. A capacity of ~175 mA h g⁻¹ (theoretical value) at a 1 C rate was achieved, and it even reached ~100 mA h g⁻¹ at a high discharge rate of 10 C with a high cycling stability. It is a promising method for the synthesis of LTO with high rate performance and a high cycling stability.

2.6 Other methods

2.6.1 Spray pyrolysis. Spray pyrolysis is a ceramic powder processing technique for the preparation of particles through decomposition of the precursor molecules at high temperatures.¹¹² A typical spray pyrolysis system consists of a reservoir for the precursor solution, a droplet generator, reactor and a collection unit. The precursor solutions are firstly atomized and carried using gas into a reactor in which the droplets are evaporated and decomposed into solid particles. The nucleation and growth of the monomer precursors are also involved in

the process of particle formation. Electrical heating or a flame provide heat for the evaporation of the solvent and the decomposition of the precursors.¹¹³ Ju and co-workers reported a spray pyrolysis method for the synthesis of LTO.^{114–116} The precursor solution was prepared by dissolving a stoichiometric amount of lithium nitrate and titanium(IV) tetra(isopropoxide) in distilled water. The as-prepared powders obtained, using spray pyrolysis at a preparation temperature of 800 °C, were post-treated in a box furnace at temperatures ranging between 600 and 1000 °C for 12 h in air.¹¹⁴

2.6.2 Modified rheological phase method. The modified rheological phase method is a simple and inexpensive approach to synthesize spinel-LTO nanosize particles by avoiding multiple steps and complex reaction conditions. Such a method is able to overcome the impure products obtained using the conventional solid-state reaction method.¹¹⁷ Yin and co-authors¹¹⁷ reported that the initial discharge capacity of the spinel-LTO electrode material obtained using the modified rheological phase method, is 176.7 mA h g⁻¹ at 1 C, and 140.2 mA h g⁻¹ at 10 C in the voltage range between 1.0 and 3.0 V. The discharge capacities of 161.6, 156.5 and 112.3 mA h g⁻¹ were measured after 50 cycles at current rates of 1, 2.5 and 10 C, respectively.

2.6.3 Cellulose-assisted combustion synthesis. The cellulose-assisted combustion synthesis technique has the advantages of both the solid-state reaction and the sol-gel method, *i.e.*, simple synthesis, low-temperature calcination, cheap starting materials and good electrochemical performance at high charge-discharge rates.¹¹⁸ Yuan and co-authors¹¹⁸ reported a high cycling performance of LTO using the cellulose-assisted combustion synthesis. During the 50 discharge-charge cycles between 1.0 and 3.0 V from 1 to 40 C, the LTO samples demonstrated a remarkably stable rate capacity.

Beside the above-mentioned methods, other methods have also been developed; including a reflux method,¹¹⁹ a continuous flow supercritical method,⁹¹ and a sonochemical method.¹²⁰ Doi and co-authors¹²¹ first reported the preparation of uniform nanosize LTO particles using an electrospray deposition method. The spinel-LTO particles have a fairly uniform particle size of ~12 nm with a distinct crystal structure. Ernst and co-authors¹²² used the flame spray pyrolysis (FSP) to synthesize spinel-LTO with primary crystallite sizes of 7–30 nm and a high temperature stability. It has been found that the FSP process optimization could be used to further remove impurities. Moreover, FSP-prepared LTO nanoparticles showed a good sintering stability at elevated temperatures and the scalability of the process.

3. Approaches to improve performance

3.1 Lattice ion-doping of LTO

As mentioned previously, since the oxidation state of Ti in spinel-LTO is the highest possible valence (+4), spinel-LTO is a very poor electronic conductor, which leads to a low specific capacity and poor capabilities at high rates. To overcome this

drawback, great efforts have been made to increase the electrical conductivity of LTO.

3.1.1 Metallic ion doping of LTO. Metallic ion doping has been considered to be an effective way to improve the high-rate discharge capacity and cycling stability through an increase in the lattice electrical conductivity and lithium diffusion coefficient, which can be obtained by doping a cation with a higher oxidation state into the tetrahedral 8a Li^+ site or the octahedral 16d Ti^{4+} site in the LTO anode,¹²³ which then forces the partial transformation of Ti^{4+} into Ti^{3+} to generate a mixture ($\text{Ti}^{3+}/\text{Ti}^{4+}$) as charge compensation and increases the concentration of electrons.¹²⁴ For example, doping of Zn^{2+} into the tetrahedral Li^+ 8a sites or of V^{5+} into the octahedral 16d Ti^{4+} sites can effectively increase the electronic conductivity of LTO.^{125,126}

A first-principle theoretical approach has been used to calculate the electronic structure of the M-doped LTO (M = Cr, Fe, Ni, Mg).⁴¹ It has been found that both Cr and Mg doping improve the electronic conduction of LTO, while Fe or Ni doping is not beneficial for enhancing the electronic conductivity.

Doping with a variety of metal cations including Ag^+ , Sn^{2+} , K^+ , Mg^{2+} , Ca^{2+} , Zn^{2+} , Al^{3+} , Ga^{3+} , Cr^{3+} , Co^{3+} , La^{3+} , Y^{3+} , Zr^{4+} , Ru^{4+} , Mo^{4+} , Mn^{4+} , V^{5+} , Ta^{5+} , Nb^{5+} , Sr^{2+} and Cu^{2+} into the Li^+ and Ti^{4+} sites^{45,64,123–159} has been investigated extensively, and the structural properties such as ion valence and distribution, and conduction characteristics were systematically reported. Doping has been realized as an effective way to greatly improve the kinetics of the LTO anode materials in terms of discharge capacity delivery, cycling stability and, especially, rate capability. Several reports of doping LTO with metal cations are highlighted here. Gao and co-workers⁴⁵ first reported spherical La^{3+} -doped LTO powders with a high tap density synthesized using an outer gel method. The results indicate that the electrochemical performance has been improved by doping La^{3+} into LTO. The initial discharge capacity is 161.5 mA h g^{−1} at a 0.1 C rate, and the capacity still reaches 135.4 mA h g^{−1} after 50 cycles. Yi and co-workers¹²⁸ reported a micro-sized $\text{Li}_4\text{Ti}_{5-x}\text{La}_x\text{O}_{12}$ ($0 \leq x \leq 0.2$) particle synthesized using a simple solid-state method in air. The electronic conductivity and lithium diffusion coefficient of the La-modified LTO were improved. Compared with the V-doped LTO materials such as the $\text{Li}_4\text{Ti}_{5-x}\text{V}_x\text{O}_{12}$ reported by other researchers, Yu and co-authors¹²⁶ have prepared a new sample of the V-doped LTO materials by a simple solid-state reaction method; this is typical $\text{Li}_4\text{Ti}_{4.9}\text{V}_{0.1}\text{O}_{12}$. An electrochemical impedance spectrum (EIS) indicates that $\text{Li}_4\text{Ti}_{4.9}\text{V}_{0.1}\text{O}_{12}$ has a faster lithium-ion diffusivity than pristine LTO. The $\text{Li}_4\text{Ti}_{4.9}\text{V}_{0.1}\text{O}_{12}$ exhibits a discharge capacity of 117.3 mA h g^{−1} at a 5 C rate. Wolfenstine and the co-authors¹²³ reported Ta-doped LTO in the form $\text{Li}_4\text{Ti}_{4.95}\text{Ta}_{0.05}\text{O}_{12}$ synthesized using a solid-state method. Ta doping does not affect the lattice structure and particle morphology. The substitution of the Ti sites by Ta can enhance the electronic conductivity of LTO *via* the generation of a mixed $\text{Ti}^{4+}/\text{Ti}^{3+}$ species, which leads to a remarkably high cycling stability at a high charge-discharge rate. $\text{Li}_4\text{Ti}_{4.95}\text{Ta}_{0.05}\text{O}_{12}$ exhibits excellent discharge capacities of 116.1 mA h g^{−1} at 10 C and even 91.0 mA h g^{−1} at 30 C. Bai and co-authors¹⁴² first reported yttrium-doped LTO fabricated using a co-precipitation method

followed by a simple sintering process. The results show that Y-modified LTO exhibits a long-term cycling stability over more than 1000 cycles at a high current rate of 10 C, which is ascribed to the increased lattice constant, and the improved electronic and ionic conductivities arising from the Y doping. Li and co-authors¹⁴⁵ reported Zr-doped LTO prepared using a solid-state reaction under an air atmosphere. Zr^{4+} doping was found to reduce the particle size to less than 100 nm and effectively avoid particle agglomeration, contributing to the improvement in rate capability. The optimal composition of $\text{Li}_4\text{Ti}_{4.9}\text{Zr}_{0.1}\text{O}_{12}$ yielded a desirable rate capability by maintaining a discharge capacity of 118 mA h g^{−1} at 20 C. Tian and co-workers¹⁵⁰ reported niobium-doped lithium titanate with a composition of $\text{Li}_4\text{Ti}_{4.95}\text{Nb}_{0.05}\text{O}_{12}$ prepared using a sol-gel method. The $\text{Li}_4\text{Ti}_{4.95}\text{Nb}_{0.05}\text{O}_{12}$ exhibits a high rate capacity with reversible capacities of 135 mA h g^{−1} at 10 C, 127 mA h g^{−1} at 20 C and 80 mA h g^{−1} at 40 C. It can be ascribed to the higher electronic conductivity and the faster lithium-ion diffusivity by Nb^{5+} doping. Cai and co-workers¹⁵⁴ reported that controlled Al^{3+} doping into the tetrahedral 8a Li^+ sites will promote the reduction of Ti^{4+} to Ti^{3+} to increase the electronic conductivity of Al-doped LTO, which then showed a better electrochemical performance than the pure LTO anode. Zhu and co-workers¹⁵⁵ reported the spinel-type electrode materials $\text{Li}_{4-x}\text{Mg}_x\text{Ti}_5\text{O}_{12}$ ($x = 0.05, 0.1, 0.15, 0.2$) synthesized using a solid-state reaction to improve the electrochemistry and cycle performance. The results show that the electrochemical properties and cycle performance of the Mg^{2+} -doped LTO materials are improved. Zhang and co-workers¹⁵⁶ first reported zinc-doped LTO synthesized using the solid-state route. Zn doping is favorable to improve the conductivity and rate performance of LTO.

Huang and co-workers¹⁵⁷ also reported that the high-rate discharge capacity and the cycling stability of pristine LTO was significantly improved using Cu doping. The cycling behavior of a Cu-doped LTO composite was studied. As summarized in Table 4, the Cu-doped LTO composite remarkably showed a better reversible capacity and cycling stability than the pristine LTO at high charge-discharge rates.

3.1.2 Non-metallic ion doping of LTO. Some studies of anions doped into the O sites of the LTO anode, including Br^- , Cl^- and F^- , have been reported.^{133,160–163} For example, Qi and co-authors¹⁶¹ reported a Br^- -doped LTO anode in the form

Table 4 Comparison of discharge capacities and cycling stabilities of LTO and Cu-doped LTO anode materials¹⁵⁷

Rate (C)	Anode materials	Discharge capacity (mA h g ^{−1})/cycle	
		1st	10th
1	LTO	180.6	164.2
	Cu-doped LTO	209.2	171
2	LTO	162.2	155
	Cu-doped LTO	184.8	166.6
4	LTO	150.7	117.3
	Cu-doped LTO	173.4	153.6
8	LTO	98.9	72.5
	Cu-doped LTO	165.7	144.6
10	LTO	80.3	61.2
	Cu-doped LTO	142.5	141.6

of $\text{Li}_4\text{Ti}_5\text{O}_{12-x}\text{Br}_x$ ($0 \leq x \leq 0.3$), synthesized using a solid-state reaction method. The substitution of the O^{2-} sites by Br^- can increase the ratio of $\text{Ti}^{3+}/\text{Ti}^{4+}$ due to charge compensation, and it thus not only decreases the charge transfer resistance of $\text{Li}_4\text{Ti}_5\text{O}_{12-x}\text{Br}_x$ but also speeds up the diffusion rate of the lithium ions. $\text{Li}_4\text{Ti}_5\text{O}_{12-x}\text{Br}_x$ ($x = 0.2$) exhibits the largest discharge capacity among all doped samples, and shows a better reversibility and a higher cycling stability compared with the pristine LTO anode, especially at high current rates.

Huang and co-authors¹⁶² synthesized $\text{Li}_4\text{Ti}_5\text{O}_{12-x}\text{Cl}_x$ ($0 \leq x \leq 0.3$) compounds successfully via high temperature solid-state reaction. The results showed that the $\text{Li}_4\text{Ti}_5\text{O}_{12-x}\text{Cl}_x$ ($0 \leq x \leq 0.3$) compounds have a well-crystallized pure spinel phase. The $\text{Li}_4\text{Ti}_5\text{O}_{11.8}\text{Cl}_{0.2}$ sample presented the best discharge capacity among all the samples and showed better reversibility and higher cycling stability compared with pristine LTO. When the discharge rate was 0.5 C, the $\text{Li}_4\text{Ti}_5\text{O}_{11.8}\text{Cl}_{0.2}$ sample

presented a superior discharge capacity of $148.7 \text{ mA h g}^{-1}$, while that of pristine LTO was $129.8 \text{ mA h g}^{-1}$. Ma and coauthors¹⁶³ reported carbon-encapsulated F-doped LTO (C-FLTO) composites obtained using solid-state lithiation at high temperatures. The F-doping of LTO not only increased the electron conductivity of LTO through trivalent titanium (Ti^{3+}) generation, but also increased the robustness of the structure towards repeated lithiation and de-lithiation. The best-performing C-FLTO composite delivered a satisfactory performance with a high charge capacity of 158 mA h g^{-1} at a 1 C rate with negligible capacity fading after 200 cycles and an extremely high rate performance up to 140 C. A brief summary of some representative LTO anodes doped with typical cations and anions is shown in Table 5.

3.1.3 Co-doping of LTO. Several research groups have investigated how to enhance the electronic conductivity of the spinel-LTO anode materials using co-doping. Shenouda

Table 5 Summary of representative LTO doped with various cations/anions in the Li, Ti, and O sites

Doped LTO	Synthesis methods	Electrochemical performance	Advantages
Cation doping in the Li sites			
Mg-doped ¹³⁰	• Solid-state reaction with stoichiometric mixtures of $\text{Mg}(\text{OH})_2$, TiO_2 and $\text{LiOH}\cdot\text{H}_2\text{O}$	• Rate property improved	• $\text{Li}_{4-x}\text{Mg}_x\text{Ti}_5\text{O}_{12}$ increases the conductivity by many orders of magnitude
$\text{Li}_{4-x}\text{Mg}_x\text{Ti}_5\text{O}_{12}$	• @1000 °C/ H_2/He for 5 h	• 3% Mg-doped LTO has the best discharge capacity (149 mA h g^{-1}) at 0.1 C	
Ca-doped ¹⁵⁸	• Solid-state reaction with stoichiometric mixtures of Li_2CO_3 , TiO_2 and CaO	• $\text{Li}_{3.9}\text{Ca}_{0.1}\text{Ti}_5\text{O}_{12}$ exhibits the best high-rate performance	• Ca-doped LTO shows very high rate capability and excellent stability and reversibility
$\text{Li}_{4-x}\text{Ca}_x\text{Ti}_5\text{O}_{12}$	• @850 °C/air for 12 h	• Discharge capacity is $138.7 \text{ mA h g}^{-1}$ at 10 C after 100 cycles	
Al-doped ¹⁵⁹	• Solid-state reaction with stoichiometric mixtures of $\text{LiOH}\cdot\text{H}_2\text{O}$, TiO_2 and Al_2O_3	• Good cycling stability at 0.5, 1 and 2 C	• Cycling stability at high rate increased significantly
$\text{Li}_{4-x}\text{Al}_x\text{Ti}_5\text{O}_{12}$	• @ 800 °C/Ar for 5 h	• An optimal composition is $\text{Li}_{3.9}\text{Al}_{0.1}\text{Ti}_5\text{O}_{12}$	
Cation doping in the Ti sites			
V-doped ¹⁴⁸	• Solid-state method with stoichiometric mixture of TiO_2 , Li_2CO_3 and V_2O_5	• $\text{Li}_4\text{Ti}_{4.9}\text{V}_{0.1}\text{O}_{12}$ has the highest discharge capacity	• No effect on lattice parameter
$\text{Li}_{4}\text{Ti}_{5-x}\text{V}_x\text{O}_{12}$	• @ 850 °C/air for 24 h	• $\text{Li}_4\text{Ti}_{4.9}\text{V}_{0.1}\text{O}_{12}$ has a discharge capacity of 229 mA h g^{-1} after 130 cycles	• Improved reversible capacity
Zr-doped ¹⁴⁵	• Solid-state reaction using stoichiometric mixture of $\text{CH}_3\text{COOLi}\cdot 2\text{H}_2\text{O}$, TiO_2 and $\text{Zr}(\text{NO}_3)_4\cdot 5\text{H}_2\text{O}$	• $\text{Li}_4\text{Ti}_{4.9}\text{Zr}_{0.1}\text{O}_{12}$ exhibited the best rate capability	• Good cycling performance • Improved electronic conductivity and Li-ion diffusivity
$\text{Li}_{4}\text{Ti}_{5-x}\text{Zr}_x\text{O}_{12}$	• @800 °C/air for 10 h	• $\text{Li}_4\text{Ti}_{4.95}\text{Nb}_{0.05}\text{O}_{12}$ has a higher specific capacity and better cycling performance	• Better rate capability • Improved electronic conductivity and Li-ion diffusivity
Nb-doped ¹⁵⁰	• Sol-gel method with stoichiometric amounts of CH_3COOLi , $\text{Ti}(\text{OC}_4\text{H}_9)_4$ and $\text{Nb}(\text{OH})_5$	• Specific capacities of $169.1 \text{ mA h g}^{-1}$ at 1 C and $115.7 \text{ mA h g}^{-1}$ at 10 C even after 100 cycles	• Better rate capability
$\text{Li}_{4}\text{Ti}_{5-x}\text{Nb}_x\text{O}_{12}$	• Gel dried at 120 °C for 10 h • @ 800 °C/Ar for 12 h		• Good crystallinity and high phase purity
Anions doping in the O site			
Br-doped ¹⁶¹	• Solid-state reaction using stoichiometric mixture of $\text{LiOH}\cdot\text{H}_2\text{O}$, $\text{LiBr}\cdot\text{H}_2\text{O}$, and TiO_2	• $\text{Li}_4\text{Ti}_5\text{O}_{11.8}\text{Br}_{0.2}$ presented the highest discharge capacity 172 mA h g^{-1} , and $150.2 \text{ mA h g}^{-1}$ after 50 cycles at 0.5 C rate	• $\text{Li}_4\text{Ti}_5\text{O}_{11.8}\text{Br}_{0.2}$ showed promising anode material for lithium-ion batteries
$\text{Li}_4\text{Ti}_5\text{O}_{12-x}\text{Br}_x$	• @900 °C /air for 12 h	• The $\text{Li}_4\text{Ti}_5\text{O}_{11.8}\text{Cl}_{0.2}$ presented the best discharge capacity, better reversibility.	• Increased the specific capacity significantly
Cl-doped ¹⁶²	• Solid-state reaction using stoichiometric mixture of	• Superior discharge capacity of $148.7 \text{ mA h g}^{-1}$	• Doped Cl^- can increase the amount of $\text{Ti}^{3+}/\text{Ti}^{4+}$ mixing charge • Improved the lithium-ion diffusion.
$\text{Li}_4\text{Ti}_5\text{O}_{12-x}\text{Cl}_x$	• $\text{LiOH}\cdot\text{H}_2\text{O}$, $\text{LiCl}\cdot\text{H}_2\text{O}$, and anatase-TiO ₂ • @800 °C/air for 12 h		

and co-authors⁶⁴ reported the anode materials $\text{Li}_{4-x}\text{Mg}_x\text{Ti}_{5-x}\text{V}_x\text{O}_{12}$ ($0 \leq x \leq 1$) for lithium-ion batteries synthesized using solid-state reaction. The addition of Mg^{2+} and V^{5+} ions improves the conductivity of the material as observed in $\text{Li}_{3.25}\text{Mg}_{0.75}\text{Ti}_{4.25}\text{V}_{0.25}\text{O}_{12}$, which shows a higher electrical conductivity and specific discharge capacity, as well as a longer cycle life than the other samples. Wang and co-authors¹³⁸ reported Ni^{2+} and Mn^{4+} co-doped spinel LTO materials prepared using the sol-gel route and calcination under an air atmosphere. The results show that the co-doped LTO samples with different molar fractions of Ni and Mn ions exhibit an enhanced electrochemical performance even at high current rates. The $\text{Li}_4\text{Ti}_{4.8}\text{Ni}_{0.1}\text{Mn}_{0.1}\text{O}_{12}$ sample, in particular, exhibits a relatively good rate capability with an initial discharge capacity of $172.4 \text{ mA h g}^{-1}$.

With respect to the co-doping method, further insights into structural alternations, interface characteristics, interactions between the co-doping ions and the matrix as well as into the resulting ion distributions are still necessary to evaluate the complicated effects of co-doping on the electrochemical properties of LTO.

3.1.4 Metal oxide-doping of LTO. So far, several studies of metal oxide-doped LTO have been reported. Huang and co-authors¹⁶⁴ reported that the Cu_xO -doped LTO composite anode materials exhibit much better rate discharge capacities and cyclabilities than pristine LTO. The discharge capacity of the composite remains $137.6 \text{ mA h g}^{-1}$ after 100 cycles at 10 C . Wang and co-authors¹⁶⁵ reported an initial discharge capacity of 476 mA h g^{-1} and a specific capacity of 236 mA h g^{-1} after 16 cycles in SnO_2 -doped LTO composites prepared using a solution method. SnO_2 acts as a bridge between the spinel particles to reduce the interparticle resistance and is a good material for Li insertion. The specific capacities of the composite material are larger than the weighted sums of the capacities of pure SnO_2 and LTO, indicating the presence of synergistic interactions between the two materials. TiO_2 is another promising dopant for improving the capacity of LTO. Rahman and co-authors¹⁶⁶ reported a nanocrystalline LTO- TiO_2 duplex phase synthesized using a simple basic molten-salt process using a eutectic mixture of LiNO_3 - LiOH - Li_2O_2 . A heat-treatment at $400 \text{ }^\circ\text{C}$ for 3 h yielded the best electrochemical performance in terms of charge-discharge capacity and rate capability. It shows initial discharge capacities of 193 mA h g^{-1} at 0.2 C , 168 mA h g^{-1} at 0.5 C , 146 mA h g^{-1} at 1 C , 135 mA h g^{-1} at 2 C , and 117 mA h g^{-1} at 5 C . After 100 cycles, the discharge capacity is 138 mA h g^{-1} at 1 C with a capacity retention of 95%. Its superior electrochemical performance can be mainly attributed to the duplex crystallite structure, composed of fine ($< 10 \text{ nm}$) and coarse ($> 20 \text{ nm}$) nanoparticles, where lithium ions can be stored within the grain boundary interfaces between the spinel-LTO and the anatase- TiO_2 .

It should be pointed out that the conductivity and electrochemical performance of LTO can be improved by doping with some cations and anions. However, it is not feasible to prepare the doped-LTO anode for large scale commercial production. In addition, some ion doping in LTO has demonstrated that the high-rate performances are far from reaching satisfactory common values and further research efforts are still needed.

Hence, the research community is still looking for an alternative approach to improve the conductivity and electrochemical performance of LTO using some other techniques and methods.

3.2 Nanostructured LTO

One of the widely used chemical strategies is to synthesize nanostructured LTO materials with various nanoarchitectures such as nanorods, nanowires, and nanotubes.^{167–170} In this strategy, the electronic conductivity and Li^+ ion diffusion coefficient are essentially unchanged. Particularly, these LTO nanostructures can facilitate both the electron and lithium ion transport by reducing their transportation pathways within the LTO particles, and also improve the intercalation kinetics by providing a larger electrode/electrolyte contact area.^{171–174} Several typical nanostructures, including one-dimensional, two-dimensional, and three-dimensional LTO materials, have been prepared and summarized herein.

3.2.1 One-dimensional LTO. Jo and co-authors¹⁷⁵ have fabricated LTO nanofibers using an electrospinning method. The diameters of these nanofibers could be controlled to be $200\text{--}600 \text{ nm}$. The nanofiber type of nanoarchitecture could shorten the electron and Li^+ ion transport distance, leading to high rate performance of LTO. At 10 C , they showed a large capacity of 138 mA h g^{-1} at $1.0\text{--}3.0 \text{ V}$. Wang and co-authors¹⁷⁶ reported that the porous LTO nanofibers had an average diameter of 230 nm and were composed of nanoparticles with an average diameter of 47.5 nm . Structures like the porous LTO nanofibers showed excellent rate performance with a reversible capacity of 120 mA h g^{-1} at 10 C at $1.0\text{--}2.0 \text{ V}$.

3.2.2 Two-dimensional LTO. Hong and co-authors¹⁷⁷ synthesized ultrathin LTO nanosheets using a hydrothermal route using ultrathin titanate nanowires as the precursor. The as-synthesized LTO nanosheets have a large surface area of $159.2 \text{ m}^2 \text{ g}^{-1}$ and their thickness was found to be $5\text{--}7 \text{ nm}$. Consequently, these LTO nanosheets exhibited excellent rate performance, and delivered a large reversible capacity of 150 mA h g^{-1} at 1 C at $1.0\text{--}2.5 \text{ V}$.

3.2.3 Three-dimensional LTO. Yu and co-authors¹⁷² synthesized mesoporous LTO hollow spheres with high quality using a template approach. These spheres had mesoporous shells with tunable thicknesses. Benefiting from the unique structural features, these spheres exhibited advanced rate performance with a reversible capacity of 115 mA h g^{-1} at 10 C at $1.0\text{--}3.0 \text{ V}$. He and co-authors¹⁷⁸ prepared monodispersed LTO hollow spheres using carbon spheres as a template. The LTO hollow spheres had an average outer diameter of $1.0 \mu\text{m}$ and an average wall thickness of 60 nm . As a result, they exhibited favorable rate performance with a specific capacity of 100 mA h g^{-1} at 10 C at $1.0\text{--}3.0 \text{ V}$. Shao and co-authors¹⁷⁹ prepared nanoporous LTO with a sol-gel method using monodispersed polystyrene spheres as a template. The nanoporous structure had an average diameter of approximately 100 nm and a wall thickness of about 50 nm . As a result, this nanoporous LTO material showed advanced rate performance with a specific capacity of 102 mA h g^{-1} at 10 C at $0.5\text{--}3.0 \text{ V}$. Chen and co-authors⁴⁶ synthesized LTO microspheres, assembled from sawtooth-like nanosheets, using a hydrothermal process

and subsequent thermal treatment. The microspheres had diameters ranging from 400 to 600 nm, and a large specific surface area of $139.4 \text{ m}^2 \text{ g}^{-1}$. These LTO microspheres exhibited high rate performance with a reversible capacity of 135 mA h g^{-1} at 57°C at $1.0\text{--}2.5 \text{ V}$. Chou and co-authors³³ synthesized LTO microspheres using a combination of a microwave-assisted hydrothermal method and a microwave post-annealing process. The as-prepared LTO microspheres had sizes of 500–800 nm, and were composed of small nanoflakes around 10 nm thick, leading to advanced rate performance. At 20°C , this material delivered a specific capacity of about 100 mA h g^{-1} at $1.0\text{--}3.0 \text{ V}$ using carboxymethyl cellulose as a binder. Lin and co-authors¹⁸⁰ fabricated mesoporous LTO spheres using a hydrothermal method followed by calcination. The pore sizes in the mesoporous LTO spheres were about 4 nm. The mesoporous LTO exhibits a stable capacity of 140 mA h g^{-1} at 0.5 C . The reversible capacity at 30°C remained over half of that at 0.5 C . The mesoporous structure creates a rapid lithium transportation path and facilitates the rate capability. As a result, the mesoporous LTO might be a promising anode material for high-performance anodes for next-generation LIBs.

3.3 Carbon surface modification of LTO

Carbon materials have proven to be an effective means of improving the electrochemical performance of the LTO anode material due to their low cost and high conductivity. So far, tens of literature articles have reported the syntheses and electrochemical properties of various carbon–LTO anode composites. Using different carbon forms (*e.g.*, amorphous carbon, carbon nanotubes, and graphene) and carbon surface modifications on LTO, they generally promote the electron transport among the interconnected LTO particles. This process effectively enhances the electronic conductivity of such carbon–LTO composite anode materials, and thus improves the electrochemical performance in terms of rate capability, lithium storage capacity and capacity retention.^{168,181–190}

3.3.1 Amorphous carbon-coating of LTO. Carbon-coating has been shown to be an effective method to improve the electrochemical performance of the LTO anode material in LIBs. Many examples in the literature reported the syntheses and electrochemical properties of amorphous carbon-coated LTO nanostructures using various synthetic methods.^{168,181–190} When the source of the appropriate carbon form is optimized, carbon-coated LTO nanostructures with uniform coating thickness can be produced effectively.^{63,187,191–193} The optimum carbon-coating can improve not only the surface electrical conductivity but also the electrical contact between the LTO materials and the conducting agents (electrolyte), which leads to a reduction of the cell impedance and a decrease in the charge-transfer resistance. As a result, the specific capacity, rate capacity and cycling performance of an LTO battery can be greatly enhanced. However, it is difficult to define the optimum carbon content without discussing the carbon structure. If the carbon is not homogeneously distributed on the LTO particle surfaces, it is even harder to define the optimum amount of carbon content (wt%) and carbon-coating thickness. It has been proposed that an ideal LTO structure should contain nanosized particles completely coated with thinner carbon.^{182,186,187,191}

In addition, the carbon-coating thickness is generally related to the carbon content and surface area. A high carbon content can contribute to a high surface conductivity but also produce thick carbon-coating (*i.e.* up to 10 nm), which might restrict the transport of lithium ions, in which case it is thus unfavorable for attaining high rate capacities.^{194–196} Only optimized and uniform carbon-coating can provide good conductivity and fast Li-ion transport in the carbon-coated LTO materials. However, it still remains a major challenge to fabricate carbon-coated LTO materials with optimized carbon content and a desirable coating thickness using facile techniques.^{63,90,168,181,186–190,192–197} The ultimate goal in many studies is to find a simple and efficient method for the synthesis of these LTO anode materials with optimal and uniform carbon-coatings.^{182,186,187,191} An enhanced electrochemical performance can be achieved with a synergistic effect between high electric conduction and high ionic transport by optimizing the coated-carbon content and structure.^{194–198} Here, we summarize several typical studies of the effect of morphologies and structures of the carbon-coated layer on the lithium storage performance of these carbon-coated LTO composites.

Wang and co-authors¹⁶⁸ reported LTO nanoparticles with a double conductive surface modification of Ti(III) and carbon, synthesized using a facile solid-state reaction. The initial discharge capacity of the as-prepared C-LTO reaches 160 mA h g^{-1} at a current density of 0.1 A g^{-1} between 3.0 and 1.0 V , and maintains 90% of the initial capacity after 100 cycles. After the 10th cycle, the irreversible capacity almost disappears, indicating a charge-discharge efficiency of nearly 100%. Furthermore, a discharge capacity of 75 mA h g^{-1} is also achieved even at a high current density of 3 A g^{-1} (about 20 C). Cheng and co-authors¹⁸² reported a simple approach to synthesize carbon-coated nanostructured LTO with various morphologies, such as LTO nanorods, hollow spheres and nanoparticles, using a simple carbon pre-coating process. The as-synthesized LTO nanorods exhibit excellent cycling performance between 1.0 and 3.0 V at a rate of 1 C , and maintain 95% of the initial capacity after 1000 cycles. This can be ascribed to the fact that the carbon layer acts as a buffer layer to maintain a good electronic conductivity path. Wang and co-authors¹⁸⁵ reported nanocarbon-coated LTO, obtained with a solid-state reaction using the precursors TiO_2 and Li_2CO_3 with added sugar. The sugar does not affect the spinel structure, and it decreases the particle size by inhibiting the agglomeration of particles during the heat treatment. Electrochemical results show that the nanocarbon-coated LTO displays a larger diffusion coefficient for the lithium ions, a higher rate capability and excellent reversibility. Gao and co-authors¹⁸⁴ reported a spherical C-LTO composite with a high specific capacity and excellent cycling performance synthesized with a novel technique using carbon black. Yang and co-authors¹⁹⁰ reported a C-LTO composite synthesized using a simple solid-state reaction using Super-P-Li conductive carbon black as the reaction precursor. The initial reversible specific capacity of the C-LTO composite at a 0.5 C rate, cycled between 1.0 and 2.0 V , is $174.5 \text{ mA h g}^{-1}$ and after 300 cycles its value remains at $143.9 \text{ mA h g}^{-1}$.

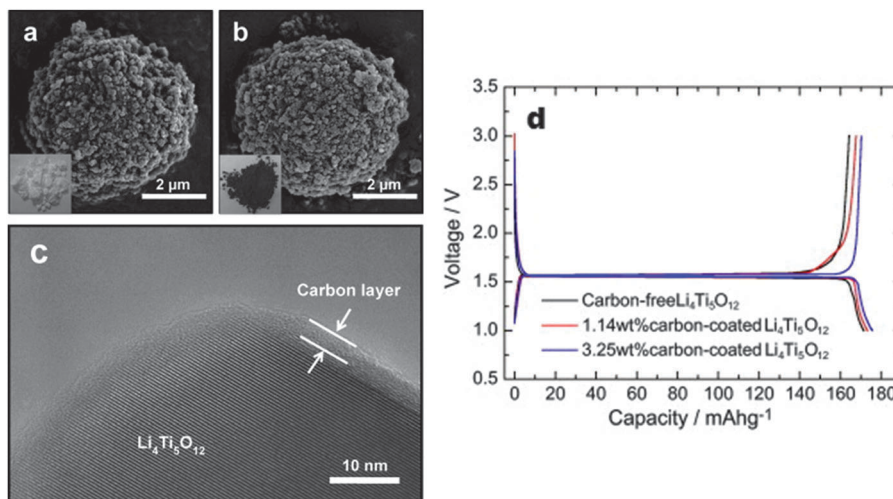


Fig. 2 SEM images of (a) carbon-free and (b) carbon-coated LTO powders. (c) High-resolution TEM image of the carbon-coated LTO. (d) Initial charge and discharge curves of carbon-free and of two different carbon-coated LTO electrodes at a rate of 0.1 C. Reproduced with permission from ref. 199. Copyright 2011 Elsevier.

Jung and co-authors¹⁹⁹ reported that spherical, high tap density, carbon-coated LTO powders were synthesized using a spray-drying process followed by a facile pitch coating. Structural analyses showed that the carbon layer uniformly coats the LTO particles without producing any crystalline changes. The carbon-coating significantly increases the electrical conductivity of LTO making it an efficient, high-rate electrode for lithium cells. The electrochemical tests in fact confirm that the 3.25 wt% carbon-coated LTO electrode operates at ultra-high rate capacity levels, *i.e.*, 100 C, and has an excellent capacity retention and charge-discharge efficiency for a life extending over 100 cycles. A comparison of structure and electrochemical performance for carbon-free and carbon-coated LTO electrodes is shown in Fig. 2.

Lin and co-authors²⁰⁰ reported the synthesis of a C-LTO anode composite using a modified one-step solid-state reaction using the original materials of lithium polyacrylate (PAALi) as the lithium and carbon source, and TiO₂ as the titanium source. The initial specific capacity of the composite is 130.0 mA h g⁻¹ at a current density of 8.60 mA cm⁻², with a capacity loss of 9.0% after 50 cycles. Liu and co-authors²⁰¹ reported a C-LTO composite synthesized at 800 °C for 15 h under argon, containing 0.98 wt% of carbon. The composite exhibits better electrochemical properties compared with the pristine LTO due to the enhanced electrical conductive network of the carbon-coating on the particle surface. The composite can deliver a capacity of 173.9 mA h g⁻¹ at a 0.1 C rate while that of pure LTO is 165.8 mA h g⁻¹ at 0.1 C. Liu and co-authors²⁰¹ reported spinel C-LTO powders synthesized successfully with a simple rheological phase method using polyvinylbutyral (PVB) as both template and carbon source. This allows the LTO particles to connect effectively with each other. Compared with pristine LTO, the surface electrical conductivity of the composite is improved significantly due to the *in situ* formation of carbon-coating, resulting in an enhanced electrochemical performance.

Guo and co-authors²⁰² reported the synthesis of three C-LTO composites with diverse carbon-coating morphologies

and structures using a simple solid-state method. The coated-structures were characterized by means of electron microscopy and Raman spectroscopy. Effects of carbon-coating on lithium storage performance, especially on the high rate capability of the C-LTO composites, were investigated. The results revealed that the porous and homogeneous carbon layer was more favorable to achieve the balance between good electron conduction and Li ion diffusion, than the island-like carbon layer and the compact one, and thus the corresponding LTO-C composites exhibited improved electrochemical performance. A schematic illustration for the effect of coated carbon on the electron conduction and Li ion diffusion within three different C-LTO composites is illustrated in Fig. 3. At a low current rate of 0.2 C, the reversible capacity of the C-LTO composite with a porous and homogeneous carbon layer, was as high as 171 mA h g⁻¹. At 5 C, the high capacity of 150 mA h g⁻¹ experienced no loss after 300 cycles. Importantly, at a high charge-discharge rate of 30 C, the reversible capacity still remained at a high level of 82 mA h g⁻¹. Due to the optimal balance between electron conduction and Li ion diffusion, the C-LTO composite with a porous and homogeneous carbon layer exhibited remarkable electrochemical properties including highly reversible capacity, superior rate capability and good cycling stability.

3.3.2 Graphene-modified LTO. Graphene, a two-dimensional macromolecular sheet of carbon atoms with a honeycomb structure, shows high electronic conductivity and attractive mechanical properties, and may in principle be an ideal conductive additive for hybrid nanostructured electrodes.^{203,204} Graphene-based materials have superior electronic conductivity compared to graphitic carbon, a high surface area of over 2600 m² g⁻¹, chemical tolerance and a broad electrochemical window, which could be very advantageous for applications in energy technologies.

Zhu and co-authors⁵⁴ reported that the as-prepared graphene-embedded LTO anode material showed improved discharging-charging and cycling properties, particularly at high rates (22 C), which makes the nanocomposite an attractive anode material

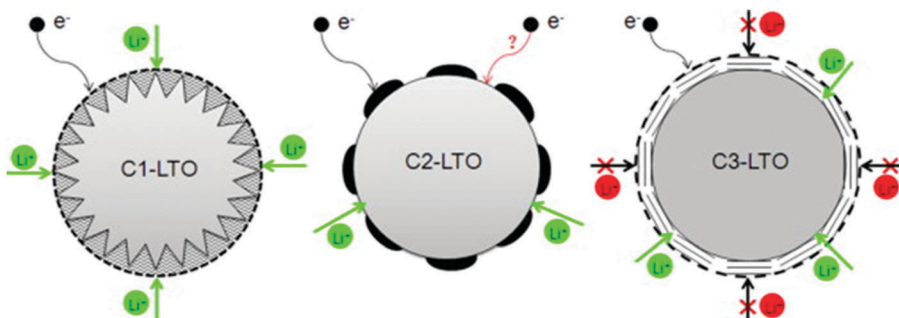


Fig. 3 Schematic illustration of the effect of coated carbon on the electron conduction and Li ion diffusion within C1–LTO (porous and homogeneous), C2–LTO (non-homogeneous), and C3–LTO (non-porous coating) composites. Reproduced with permission from ref. 202. Copyright 2014 Elsevier.

for applications in electric vehicles. Shen and co-authors²⁰⁵ developed a facile route to fabricate a composite of electrically conductive graphene nanosheets (GNS) anchored with nanocrystalline LTO as an advanced anode material for high performance LIBs. The hybrid nanostructures endow the composites with a high transportation rate for both Li⁺ and electrons (especially at high rates), because the hybrid nanostructure is capable of effectively utilising the good conductivity, high surface area, and good electrochemical performance of GNS and the good stability of the fine LTO nanoparticles. It is the synergy of these two parts that leads to a high rate capability and stable lithium storage. Shi and co-authors²⁰⁶ reported a simple strategy to prepare a hybrid of LTO nanoparticles well-dispersed on electrically conductive graphene nanosheets as an anode material for high rate LIBs. The preparation process is illustrated in Fig. 4, and the comparison of morphologies for pure nano-LTO and the nano-LTO-G hybrid is shown in Fig. 5. The authors have found that the electron transport was improved by forming a conductive graphene network throughout the insulating LTO nanoparticles. The charge transfer resistance at the particle/electrolyte interface is reduced from 53.9 Ω to 36.2 Ω and the peak currents measured using cyclic voltammetry are increased at each scan rate. The difference between the charge and the discharge plateau potentials becomes much smaller at

all discharge rates because of the lowered polarization. With 5 wt% graphene, the hybrid LTO materials deliver a specific capacity of 122 mA h g⁻¹, even at a very high charge–discharge rate of 30 C, and exhibit an excellent cycling performance with the first discharge capacity of 132.2 mA h g⁻¹ and less than 6% discharge capacity loss over 300 cycles at 20 C. The outstanding electrochemical performance of the nano-LTO-graphene hybrid makes it a promising anode material for high-rate LIBs. Oh and co-authors²⁰⁷ reported the synthesis of graphene-wrapped LTO particles using a solid-state reaction. It has been found that the LTO, tightly bound to the graphene, exhibits a remarkable specific capacity of 147 mA h g⁻¹ at a rate of 10 C (175 mA h g⁻¹ at 1 C) after 100 cycles. The improved rate capability was attributed to the enhanced electronic conductivity of each LTO grain *via* uniform graphene wrapping. Zhang and co-authors²⁰⁸ prepared an LTO-graphene composite (1.86 wt%) electrode material using both ball milling and a simple chemical method. It has been found that the composite displayed a high-rate capacity of 118.7 mA h g⁻¹ at 20 C and a good cycle stability, retaining over 96% of its initial capacity after 50 cycles at 10 C. The excellent electrochemical performance is attributed to a decrease in the charge-transfer resistance due to the fact that the LTO particles uniformly cling to the graphene sheets. Rai and co-authors²⁰⁹ reported the solvothermal preparation of LTO-graphene (15 wt% and 30 wt%)

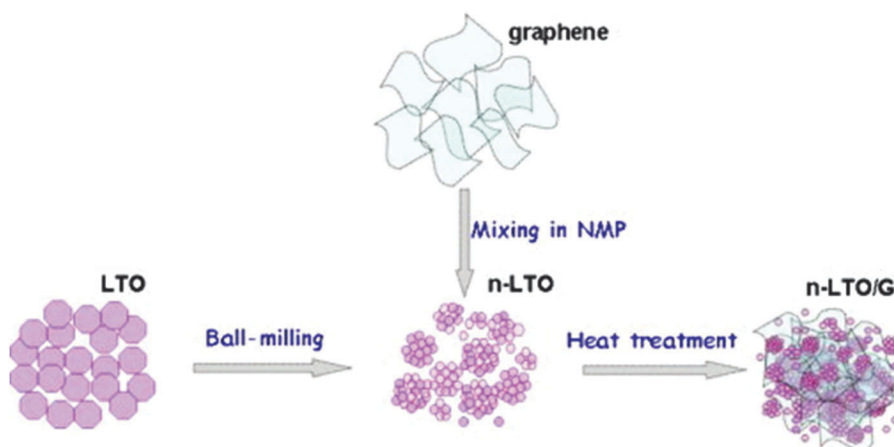


Fig. 4 Schematic representation of the preparation of the hybrid of nano-LTO and graphene. Reproduced with permission from ref. 206. Copyright 2014 Elsevier.

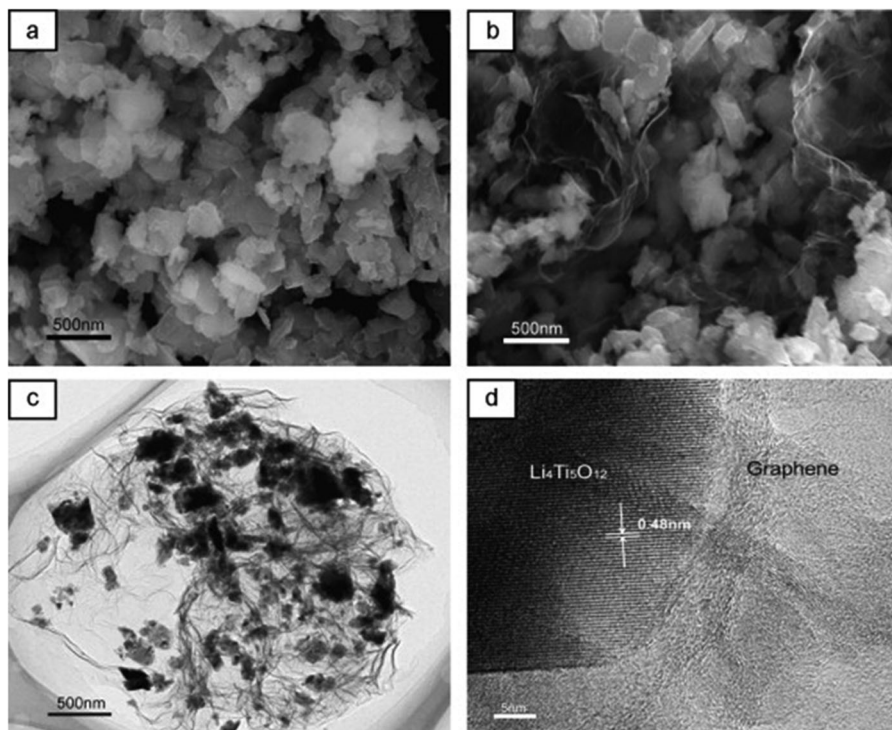


Fig. 5 SEM images of nano-LTO (a) and the nano-LTO–graphene hybrid (b). TEM (c) and HRTEM (d) images of the nano-LTO–graphene hybrid. Reproduced with permission from ref. 206. Copyright 2014 Elsevier.

nanocomposite anodes for high-performance lithium-ion batteries. Structure and morphology studies of the nanocomposites revealed that the LTO nanoparticles are embedded onto the graphene nanosheets. The electrochemical performances of the LTO–graphene nanocomposites indicate higher capacities and enhanced cycle performances within the voltage range of 1.0–2.5 V, suggesting that the LTO–graphene nanocomposite is a promising anode material for high-energy density and safe LIBs. Han and co-authors²¹⁰ reported that strongly coupled LTO-reduced graphene oxide (RGO) nanocomposites were synthesized using the solvothermal treatment of a GO colloidal suspension containing a microcrystalline LTO precursor at elevated temperatures. The solvothermal treatment of the mixture

suspension of GO and LTO gives rise not only to the reduction of GO to RGO but also to the attachment of the LTO particles to the flat surface of the RGO 2D nanosheets. The crystal structure and morphology of the LTO particles remain intact after the composite formation with the RGO nanosheets. The LTO–RGO nanocomposites display better anode performance with a larger discharge capacity of 175 mA h g⁻¹, underscoring the merit of RGO hybridization in improving the electrode performance of the bulk metal oxide, as shown in Fig. 6. The obtained LTO–RGO nanocomposites show promising electrode performance, which is superior to those of the pristine LTO microcrystals. The enhancement in electrical conductivity is mainly responsible for the observed improvement in the electrode performance

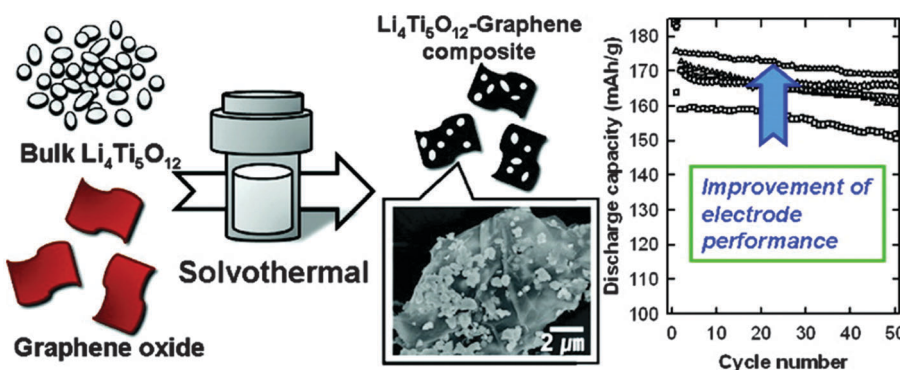


Fig. 6 Schematic illustration of the preparation of the LTO–RGO nanocomposites and graph of the improvement in electrode performance. Reproduced with permission from ref. 210. Copyright 2012 American Chemical Society.

upon composite formation with the RGO nanosheets. Pang and co-authors²¹¹ reported a mesoporous LTO-graphene hybrid synthesized using a facile electrostatic adsorption method. Such an electrostatic adsorption method is easy to scale up and will provide a new pathway for the production of various high-rate lithium-ion battery materials. The graphene sheets are strongly attached to the LTO spheres and thus can form an efficient electrically conducting network, permitting the electrode to speed up the charge and discharge processes. The as-obtained LTO-graphene nano-hybrid exhibits a high reversible capacity and outstanding rate performance owing to the synergy of good conductivity, large surface area, flexibility of graphene and good stability of the mesoporous LTO. The discharge capacity of the LTO-graphene hybrid was improved to 124 mA h g^{-1} at a 20 C rate, which is more than twice the value of the LTO electrode. Xiang and co-authors²¹² prepared a LTO-graphene composite using a facile sol-gel method. The LTP-graphene composite presents a higher capacity and better cycling performance than LTO at the cut-off of 2.5–1.0 V, especially at high current rates. The cycling stability of the cells with the electrodes using LTO and the LTO-graphene composite at 0.2 C and 10 C were investigated, the discharge capacity of LTO-graphene is slightly higher than the capacity of LTO and the specific capacity

retention during 100 cycles is 94%. At 10 C, the 100th discharge capacity of LTO-graphene is 110 mA h g^{-1} , which is much higher than that of LTO (84 mA h g^{-1}). The improvement in capacity retention especially in high rate capacity can be attributed to the introduction of superior conductive graphene. On the one hand, the graphene sheets induce the formation of fine $\text{Li}_4\text{Ti}_5\text{O}_{12}$ nanoparticles in the sol-gel synthesis. The reduced size signifies a shortened diffusion distance for the lithium ions and thus the kinetics of the lithium insertion/extraction are accelerated. On the other hand, the electronic conductivity of the $\text{Li}_4\text{Ti}_5\text{O}_{12}$ nanoparticles anchored onto the graphene sheets is significantly improved.

The excellent electrochemical performance of the LTO/graphene electrode could be attributed to the improved electronic conductivity of the graphene sheets. When discharged to 0 V, the LTO-graphene composite exhibited a quite high capacity of over 274 mA h g^{-1} below 1.0 V, which was beneficial for not only a high energy density but also the safety characteristics of lithium-ion batteries. Ri and the co-authors²¹³ reported the one-step synthesis of an LTO/graphene-ionic liquid (IL) nanostructure using a microwave-assisted hydrothermal reaction, as shown in Fig. 7, in which the ionic liquid of $\text{C}_{12}\text{H}_{23}\text{N}_2\text{Cl}$ was used as an exfoliating agent to control the microstructure of the

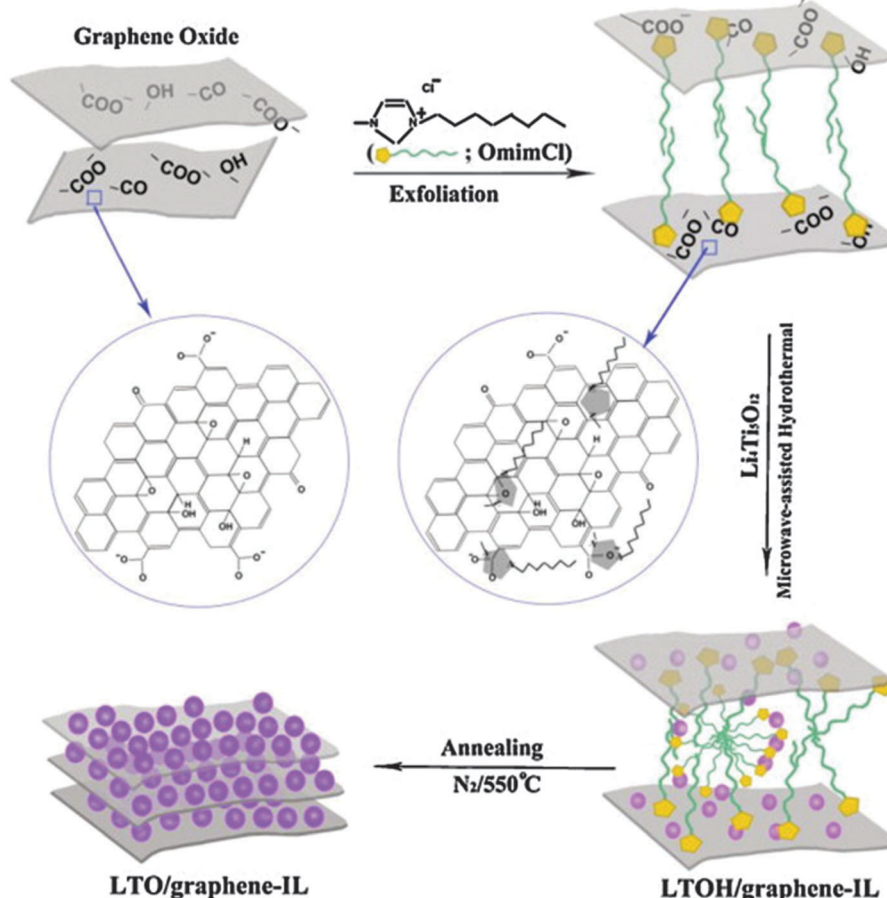


Fig. 7 Schematic representation of the preparation of the LTO/graphene-IL nanostructure from the LTO precursors, GO, and the ionic liquid using a microwave-assisted hydrothermal reaction process. Reproduced with permission from ref. 213. Copyright 2013 Elsevier.

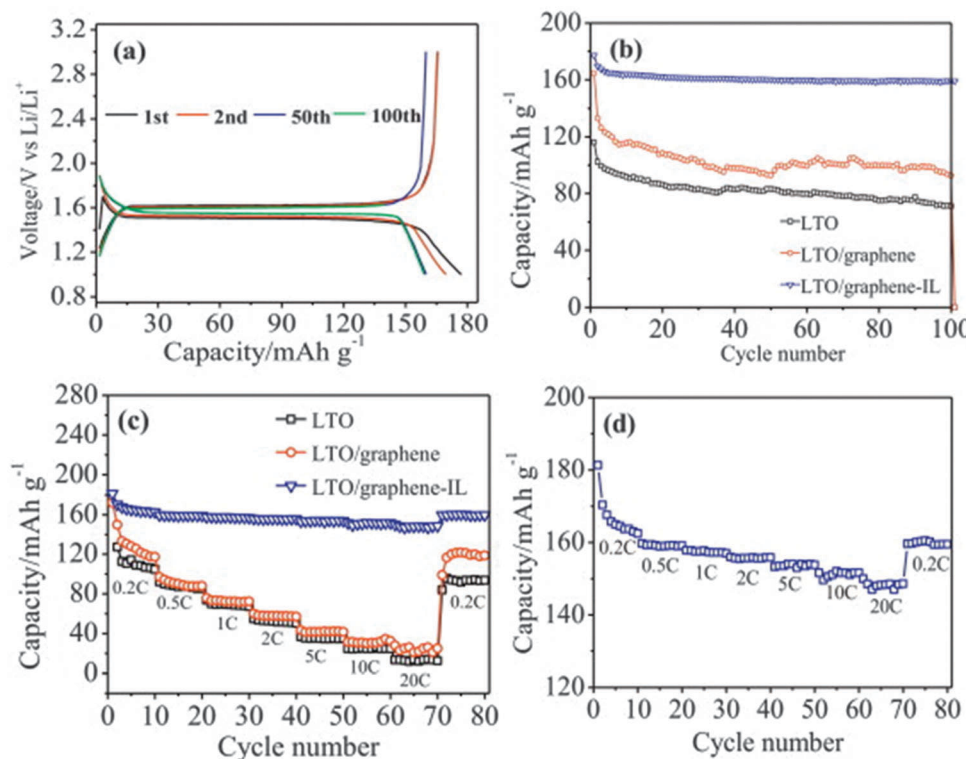


Fig. 8 (a) Galvanostatic charge–discharge profiles of the LTO/graphene–IL electrode during 1st, 2nd, 50th and 100th cycle at 0.5 C. (b) Cyclic performance of the LTO, LTO/graphene and LTO/graphene–IL electrodes at 0.5 C. (c) High-rate performance of the LTO, LTO/graphene and LTO/graphene–IL electrodes. (d) High-rate performance of the LTO/graphene–IL electrode. Reproduced with permission from ref. 213. Copyright 2013 Elsevier.

graphene sheets, and as an inducer for LTO growth on the graphene sheets. The resultant LTO/graphene–IL exhibited a two-dimensional structure with a total thickness of about 20 nm and with the LTO nanoparticles uniformly anchored on the surface of the thin graphene sheets (2 nm). Such a unique microstructure provided a high electrode/electrolyte contact area for the electron transport, and the nanosize LTO led to a short path for the lithium ion transfer. When LTO/graphene–IL was used as the anode material for a lithium-ion battery, it showed a high-rate performance, as evident from Fig. 8. The LTO-graphene nanostructure exhibits excellent reversibility (159 mA h g^{-1} at 0.5 C after 100 cycles) and high-rate performance (162 mA h g^{-1} at 0.2 C, $148.5 \text{ mA h g}^{-1}$ at 20 C).

Ni and co-authors²¹⁴ reported the preparation of LTO-reduced graphene oxide (RGO) composites using a simple strategy, as illustrated in Fig. 9. The as-prepared composites present the LTO nanoparticles uniformly immobilized on the RGO sheets. The LTO-RGO composites possess excellent electrochemical properties with a good cycle stability and high specific capacities of 154 mA h g^{-1} (at 10 C) and 149 mA h g^{-1} (at 20 C), much higher than the results found in other literature publications. The superior electrochemical performance of the LTO-RGO composites is attributed to the unique hybrid structure of the conductive graphene network with the uniformly dispersed LTO nanoparticles. Gao and co-authors²¹⁵ prepared a homogeneous LTO-graphene composite using an *in situ* solid-state

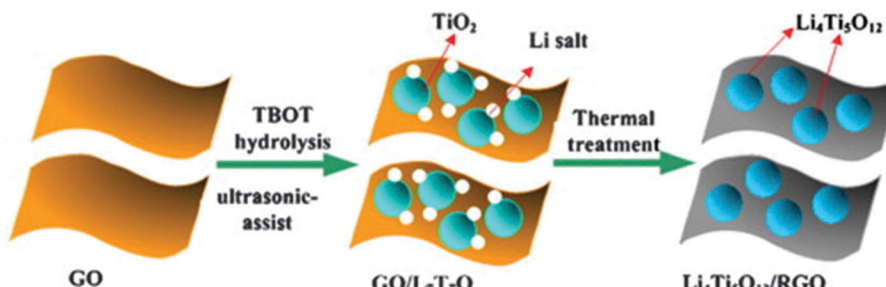


Fig. 9 Schematic representation of the fabrication process of the LTO–RGO composites. Note here: TBOT is $\text{C}_{16}\text{H}_{36}\text{O}_4\text{Ti}$. Reproduced with permission from ref. 214. Copyright 2014 Elsevier.

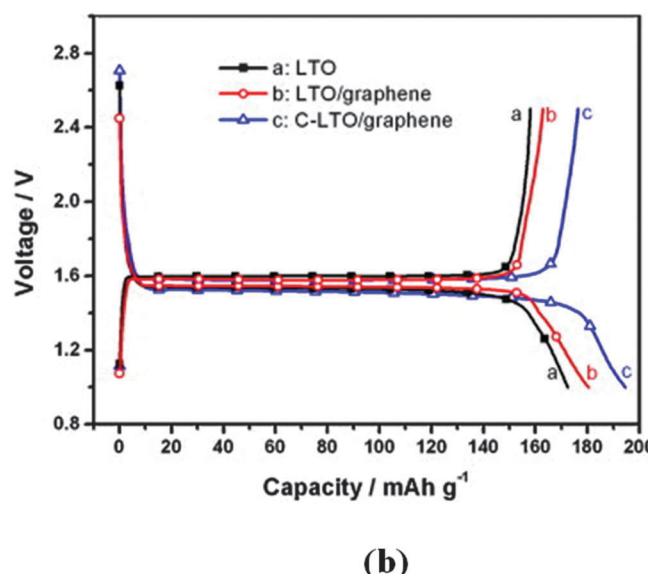
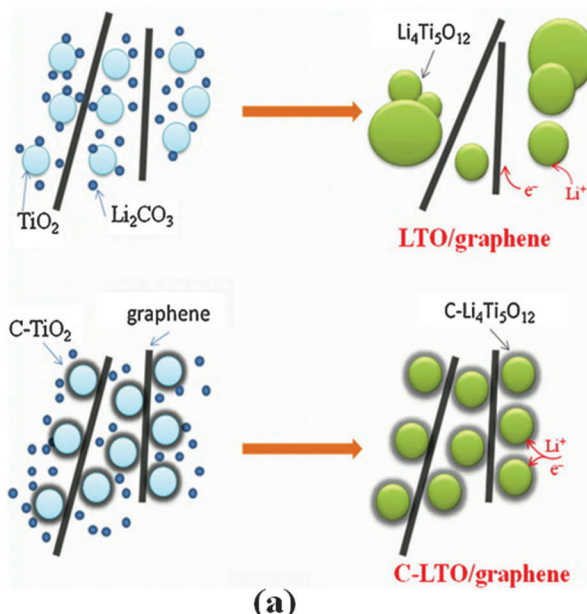


Fig. 10 (a) Schematic illustration of the effect of carbon-coating on the LTO-graphene composites. (b) Galvanostatic charge–discharge curves of the LTO, LTO-graphene, and C-LTO-graphene samples at a 0.2 C rate. Reproduced with permission from ref. 215. Copyright 2013 Elsevier.

reaction, after carbon pre-coating. Its microstructure is compared with the materials prepared using a similar method but without carbon-coating, which is illustrated in Fig. 10a. The results reveal that the carbon-coating not only effectively confines aggregation and agglomeration of the LTO particles, but also enhances the conjugation between the LTO particles and the graphene sheets. The specific capacities of the pristine LTO, the LTO-graphene composite and then carbon-LTO-graphene composite were measured by charge–discharge tests at a 0.2 C rate over the potential range of 1.0–2.5 V. It can be observed in Fig. 10b that they have similar charge and discharge plateaus, indicating that the small quantity of graphene sheets does not affect the electrochemical reaction process of LTO. All the products display very flat charge–discharge plateaus at around 1.55 V (vs. Li/Li⁺), demonstrating a characteristic two-phase reaction based on the Ti⁴⁺/Ti³⁺ redox couple. The carbon-LTO-graphene composite delivers a high reversible capacity of 177 mA h g⁻¹, which is even higher than the theoretical capacity of LTO (175 mA h g⁻¹). The increased capacity can be attributed to lithium storage on the graphene sheets. It is clear that carbon pre-coating markedly enhances the lithium storage capability of the LTO-graphene composite. The LTO-graphene composite also presents excellent rate capability and low-temperature performance. Even at 120 C, it still delivers a high capacity of about 136 mA h g⁻¹. In addition, fuel cells using LiNi_{1/3}Co_{1/3}Mn_{1/3}O₂ as the cathode material exhibit good rate capability.

3.3.3 Conducting polymer coating of LTO. Poly(3,4-ethylenedioxythiophene) (PEDOT) is a well-known conducting polymer, which is commercially used to provide conductive surfaces owing to its extraordinary electrical properties and long-term stability. Recently, Wang and co-authors²¹⁶ reported that spinel LTO nanorods coated with a PEDOT layer as an anode material for lithium-ion batteries, were synthesized using a facile soft

chemistry approach. A schematic of the synthesis is illustrated in Fig. 11. The highly conductive and uniform PEDOT layer, coated on the surface of the LTO nanorods, significantly improves the electrochemical performance of the composite, which exhibits a higher reversible capacity and better rate capability compared with the pure LTO and the LTO-C composite. As shown in Fig. 12, the reversible capacity of the LTO-PEDOT nanorods can be up to 171.5 mA h g⁻¹ at a rate of 0.2 C. Furthermore, the capacity of 168.7 mA h g⁻¹ was retained with only 0.5% capacity loss after 100 charge–discharge cycles at a rate of 1 C, which confirms the good cycling behavior of the LTO-PEDOT nanorods. The superior electrochemical performance of the LTO-PEDOT nanorods could be attributed to the one-dimensional (1D) morphology and uniform conducting polymer layer, which shortens the lithium-ion diffusion path and improves the electrical conductivity of LTO.

4. Application as anodes

A high-power energy storage device is essential for E-transportation such as electric vehicles (EVs), hybrid electric vehicles (HEVs) and plug-in hybrid electric vehicles (PHEVs). Safety is a major consideration for batteries in automotive applications. As discussed previously, the use of LTO as an anode coupled with high voltage cathodes such as LiCoO₂ (LCO), LiMn₂O₄ (LMO), or LiFePO₄ (LFP) in a high-power lithium-ion battery has been demonstrated to be feasible in terms of the electrochemical performance, such as excellent cycle life and inherent safety.^{6,217,218} It was reported that by combining the 1.5 V LTO anode with another cathode, the safety of LIBs can be significantly improved.²¹⁹ 2 V LTO/LCO (LiCoO₂) cells exhibit an excellent cycle life as is expected with lithium intercalation/de-intercalation

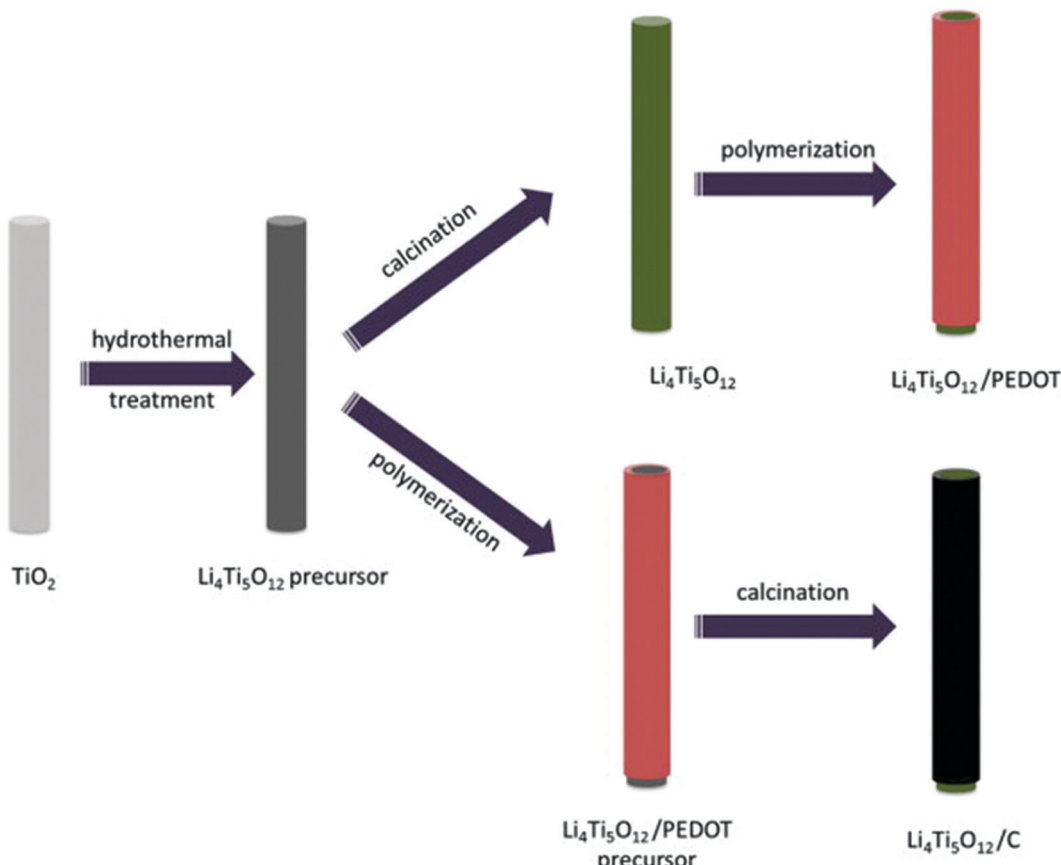


Fig. 11 Schematic illustration for the synthesis of the LTO/PEDOT and LTO/C nanorods. Reproduced with permission from ref. 216. Copyright 2014 Elsevier.

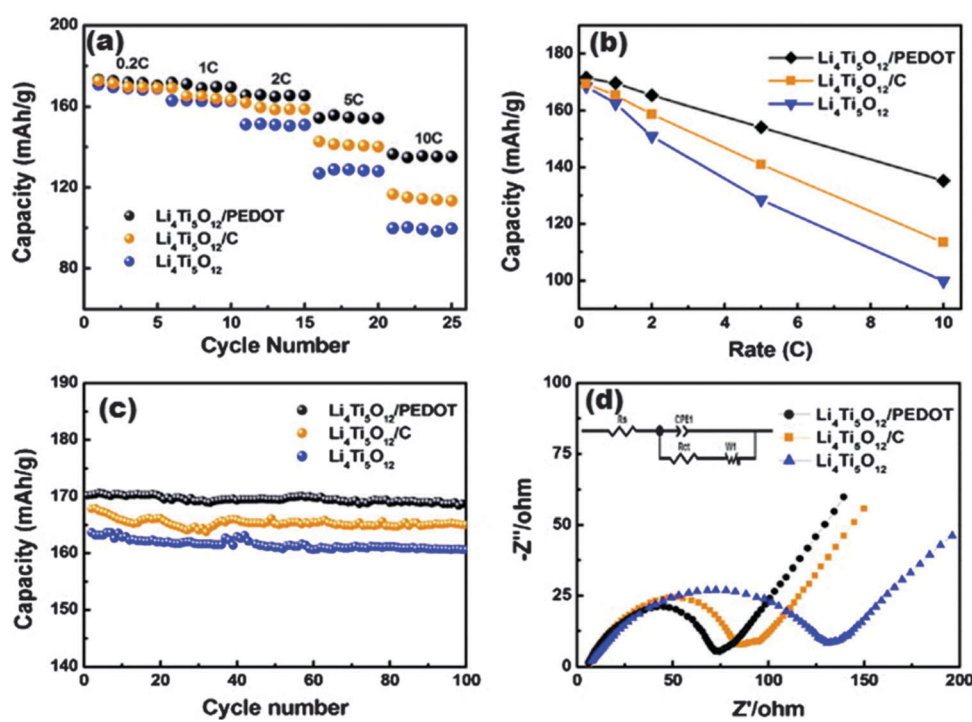


Fig. 12 (a) The rate and cycling performances at different rates. (b) Comparison of the specific capacities at different rates. (c) Cycling performance at a 1 C rate. (d) Nyquist plots of the pure LTO, LTO/PEDOT and LTO/C electrodes. Reproduced with permission from ref. 216. Copyright 2014 Elsevier.

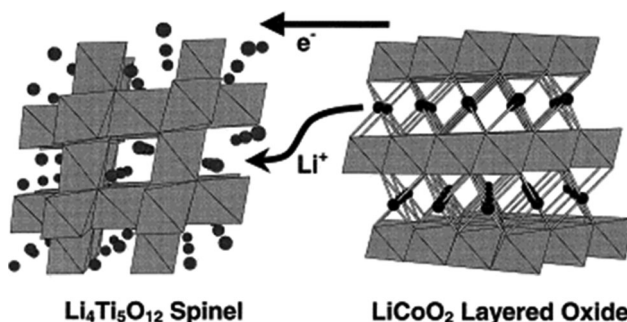


Fig. 13 Intercalation into the LTO spinel and de-intercalation out of the LCO layered structure from an LTO/LCO ideal cell couple. Reproduced with permission from ref. 28. Copyright 1999 Elsevier.

into/out of stable metal oxide structures.²⁸ In this couple, the positive and negative electrodes are based on transition metal oxide electrodes, which have the capability of accommodating a significant amount of lithium within the host electrode structure, as shown in the Fig. 13. By restricting shallow limits of charge and discharge, the structural integrity of the electrodes can be maintained, and this permits a high cycle life to be obtained with this combination.²⁸

Lu and co-authors²²⁰ reported the design of a lithium-ion cell of LTO/L333 ($\text{Li}_{1.1}\text{Ni}_{0.3}\text{Co}_{0.3}\text{Mn}_{0.3}\text{O}_2$). The cell exhibited the improved cycling performance at both room and elevated temperatures. For example, such an LTO/L333 cell at room temperature and at an elevated temperature (55 °C) had the same capacity for 30 cycles at a 10 C rate, and the capacity retention remained stable for over 200 cycles.

Bousquet and co-authors²²¹ reported good cycling performance of the Li-ion cells of 2.5 V LTO/LMO (LiMn_2O_4) with new stable Li-ion battery electrolytes such as new polyfluorinated boron cluster lithium salts. The capacity retention of such a cell was found to maintain 93% after 160 cycles at a 1 C rate at 50 °C.^{222,223}

It has been reported that 2.5 V LTO/LMO cells²²³ also showed a very promising cycling performance and a larger capacity at high current rates, which is necessary for the high current pulsing in transportation applications. These LTO/LMO cells, with capacities of $\sim 2 \text{ A h g}^{-1}$, provided new insights into the commercialization of LTO/LMO batteries.

A cell with a 2.5 V LTO-LMO system²²⁴ also showed unprecedented power capability over that of any existing lithium-ion battery system for HEV and other transportation applications. This LTO-LMO system also demonstrated good calendar life, low heat generation during high-rate operation, and excellent low-temperature (-30°C) performance, as well as unmatched abuse tolerance.

Hu and co-authors²²⁵ reported a hybrid battery-supercapacitor LTO/($\text{LiMn}_2\text{O}_4 + \text{AC}$) using an LTO anode and a $\text{LiMn}_2\text{O}_4/\text{activated carbon (AC)}$ composite cathode. It is demonstrated that the hybrid battery-supercapacitor has advantages in both high rate capability from the hybrid capacitor AC/LTO and high capacity from the secondary battery LTO/LMO. At a 4 C rate, the capacity loss in constant current mode is no more than 7.95% after 5000 cycles, and the capacity loss in constant current-constant voltage mode is no more than 4.75% after 2500 cycles.

Panero and co-authors²²⁶ also reported a new type of lithium-ion cell, based on the combination of an LTO anode with a high voltage mixed spinel solid solution $\text{Li}_2\text{Co}_{0.4}\text{Fe}_{0.4}\text{Mn}_{3.2}\text{O}_8$ cathode. This combination provides some promising features that may be used as a starting base for future development and optimization.

In recent years, Li-ion batteries based on an LTO anode have been investigated and developed for load-leveling applications, based on the favorable characteristics emphasized above, including high energy density, long cycle life, stability, and rapid charge. A great deal of research^{227–231} has been devoted to the new type of 2.5 V lithium-ion cell, based on the combination of a spinel-LTO anode with high-voltage olivine LiMnPO_4 (LMPO),²²⁸ spinel $\text{LiMn}_{0.8}\text{Fe}_{0.2}\text{PO}_4$ (LMFPO),²²⁹ spinel LiMn_2O_4 (LMO),^{223,232,233} and spinel $\text{LiMn}_{1.5}\text{Ni}_{0.5}\text{O}_4$ (LMNO)^{234,235} cathodes. The employment in load-leveling applications has been systematically explored and evaluated for these 2.5 V Li-ion battery cells, including LTO/LMPO, LTO/LMO, LTO/LMNO, and LTO/LMFPO. These Li-ion cells have demonstrated impressive stability, prolonged cycle life and excellent safety features, making them suitable for load-leveling applications. Herein, the redox activity of LTO/LMFPO during the lithiation-delithiation cycling process is shown in Fig. 14.

Sun and co-authors²³⁶ reported that commercial battery cells of 2 V LTO/LFP (LiFePO_4 -PAS (PAS, polyacence-highly conductive polymer)) showed an excellent specific capacity, high relative tap density, long cycle life, and high cycle efficiency at high current rates. It showed no attenuation after 1000 charge-discharge cycles during charging and discharging at a 1 C rate.

Zaghib and co-authors^{237,238} reported that the LFP/LTO cell has passed successfully the required battery tests for safety use in transportation. LTO/LFP Li-ion cells are safe and can support fast charge-discharge rates without any damage to the cycling life. The impact on electric cars will be important, since it is the most demanding use in terms of performance and safety. The electrochemical performance of the 2 V LTO/LFP 18650-Li-ion batteries has shown them to be fast-charging Li-ion batteries with long shelf lives for power applications in terms of safety and cycling life, which are key issues in E-transportation applications.^{30,66} The voltage *vs.* capacity curves for the 18650-cells of LFP/Li, LTO/Li, and LFP/LTO at a 24 C rate are summarized in Fig. 15.

Electric cars presented at the World Energy Council (Montréal, September 2010) were equipped with C-LFP/LTO batteries (Fig. 16). They had a weight of 680 kg, a driving range of 32 km with a top speed of 64 km h^{-1} . It has been demonstrated that the charging time was reduced to 5 min with a three-level charger in parallel (500 V, 125 A). This LFP/LTO battery cell technology has been attractive for the fast charging bus Mega Watt battery charging station for EV and PHEV and for energy storage with wind and solar energy.

Ariyoshi and co-authors²³⁹ reported the LTO anode combined with the LNMO ($\text{LiNi}_{0.5}\text{Mn}_{1.5}\text{O}_4$) cathode to assemble the 3 V LTO/LNMO cell system, and such a 3 V Li-ion cells showed that 83% of the initial capacity can be stored and delivered even after 1100 cycles, indicating the excellent cyclability and rate capability of the LTO/LNMO cells. Meanwhile, this 3 V LTO/LNMO

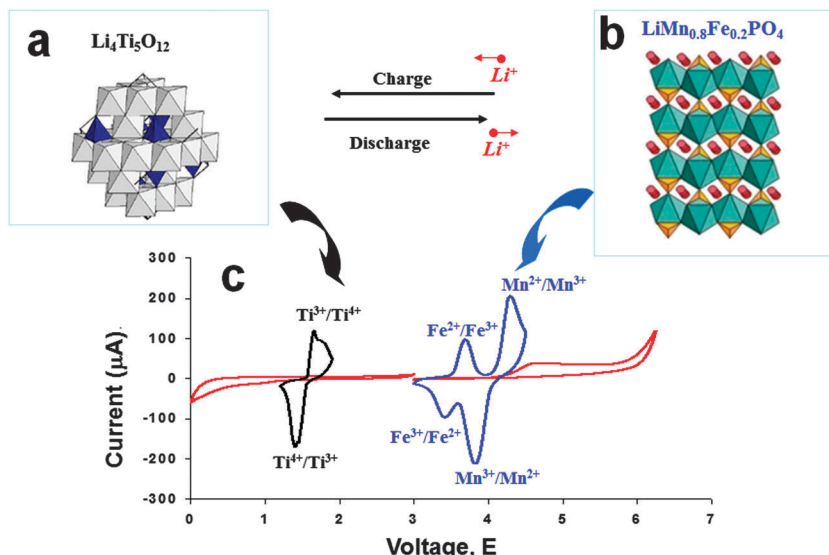


Fig. 14 Structure of the LTO spinel anode (a), and the LMFPO ($\text{LiMn}_{0.8}\text{Fe}_{0.2}\text{PO}_4$) cathode (b). (c) Schematic voltammetry response of these electrode materials in an electrolyte. Reproduced with permission from ref. 227. Copyright 2011 The Royal Society of Chemistry.

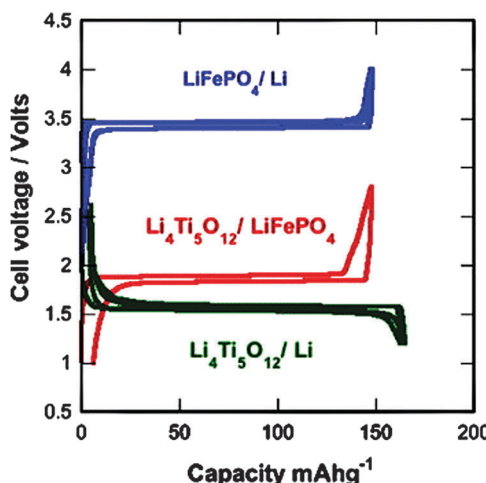


Fig. 15 Voltage–capacity cycles for the LFP/Li, LTO/Li, and LFP/LTO-18650-cells at a 24 C rate. Reproduced with permission from ref. 237. Copyright 2011 Elsevier.

cell with a dimethyl methylphosphonate (DMMP)-based electrolyte has also demonstrated an acceptable capacity loss after 30 cycles, which makes this 3 V LTO/LNMO cell promising for safe lithium-ion batteries.²⁴⁰

5. Concluding remarks and perspectives

5.1 Concluding remarks

The characteristics of the current lithium-ion batteries have greatly influenced the energy efficiency, reliability, and commercial viability for emerging applications such as high-power backup systems and electric transportation. In fact, the existing lithium-ion batteries have also impacted the reliability of many



Fig. 16 E-Cars presented at the World Energy Council (Montréal, September 2010), equipped with C-LFP/LTO battery cells. Reproduced with permission from ref. 237. Copyright 2011 Elsevier.

portable electronic tools such as smart cell phones and laptop computers. So far, lithium-ion batteries have proven to be the most viable solution for electric energy storage. However, the performances of the existing lithium-ion batteries are still not able to meet the increasing demands of these emerging

applications. The main scientific objectives are to achieve a rational design of cathode and anode materials with desired properties, such as enhanced rate capability (*i.e.* power density), high energy density, excellent structural stability, long cycling life, and reasonable costs.

This review gives a state of the art overview of spinel- $\text{Li}_4\text{Ti}_5\text{O}_{12}$ materials, which have been considered as promising anode materials for lithium-ion batteries due to their attributes of high safety and excellent rate capability.^{217,241,242} However, a number of challenges still remain in the development of $\text{Li}_4\text{Ti}_5\text{O}_{12}$ anode materials for a new generation of lithium-ion batteries to meet the emerging application criteria. Some of the major remaining challenges associated with the existing $\text{Li}_4\text{Ti}_5\text{O}_{12}$ anode materials are briefly described below.

(1) Since the improved safety of the $\text{Li}_4\text{Ti}_5\text{O}_{12}$ anode is obtained at the expense of energy density due to its high operating voltage *vs.* Li/Li^+ (~ 1.5 V), the lithium-ion battery cells with a $\text{Li}_4\text{Ti}_5\text{O}_{12}$ anode offer a low theoretical specific energy due to their low cell voltage. Therefore, lithium-ion batteries with $\text{Li}_4\text{Ti}_5\text{O}_{12}$ anodes are more likely to be used in the long term for stationary energy storage and hybrid electric vehicles in the transportation sector.

(2) Combined surface coating strategies are needed to create nano-enabled anode materials with improved electronic and ionic conductivities. The combination includes various optimized approaches such as *in situ* or *ex situ* active coating and cation or anion doping at nanometer scale. Major technical breakthroughs are needed to tackle the intrinsic insulating character without compromising safety and cost.

(3) Nanostructured $\text{Li}_4\text{Ti}_5\text{O}_{12}$ anodes, in the form of nanorods, nanowires, and porous clusters, with carbon-coatings have shown very promising performances. However, little is known about the mechanism of the elementary steps associated with charge and mass transports in the confined dimensions of the $\text{Li}_4\text{Ti}_5\text{O}_{12}$ anode (1D, 2D). More sophisticated *in situ* characterization techniques for probing and mapping those confined $\text{Li}_4\text{Ti}_5\text{O}_{12}$ surfaces are needed to gain critical insights into nanoscale phenomena on the nano- $\text{Li}_4\text{Ti}_5\text{O}_{12}$ electrode surfaces during cycling.

(4) It is important to mention that safety considerations are as important as performance, since a car accident due to electric vehicle battery safety failure may cause significant damage. High energy density also means high safety risks, and it is the responsibility of the researchers dedicated to this field to ensure that the new lithium-ion batteries meet the safety requirements before they are commercialized.

5.2 New directions

As demonstrated in this perspective review, important future directions and key research and development efforts for spinel- $\text{Li}_4\text{Ti}_5\text{O}_{12}$ anode materials for the design of advanced lithium-ion batteries are:

(1) From a scientific point of view, more fundamental studies are needed to fully understand and improve electrochemical performance (*i.e.* rate capability) of the $\text{Li}_4\text{Ti}_5\text{O}_{12}$ nanostructures using various parameters such as surface area, crystallinity, and the crystalline orientation. Compared with

traditional bulk $\text{Li}_4\text{Ti}_5\text{O}_{12}$ materials on the microscale, novel $\text{Li}_4\text{Ti}_5\text{O}_{12}$ nanostructured materials have gained more attention as high-rate anodes for rechargeable lithium-ion batteries. Owing to their small size and large surface area, the Li-ion diffusion pathway is reduced and a better contact between the $\text{Li}_4\text{Ti}_5\text{O}_{12}$ electrode material and the electrolyte is achieved. Both of these phenomena contribute to the improvement of the rate capability. In addition, more extensive studies of novel $\text{Li}_4\text{Ti}_5\text{O}_{12}$ nanoarchitecture anode materials are required. One of the strategies is to create 3D $\text{Li}_4\text{Ti}_5\text{O}_{12}$ structures combining microscale templates and nanostructures to maximize the advantages and minimize the disadvantages of the materials at the two scales. The rational design of $\text{Li}_4\text{Ti}_5\text{O}_{12}$ nanoarchitecture anodes may lead to higher energy and power densities, significantly enhancing the Li-ion battery performance. Eventually, the fundamental electrochemical kinetic behaviour (ionic or electronic) needs to be evaluated, and the critical factors of lithium intercalation and extraction (*e.g.*, nanostructure size, phase coating, doping, morphology, composition, and mixed valence conduction) need to be investigated systematically.

(2) From a practical point of view, the precursor materials' availability and cost, a cost-effective synthesis, an improved service life and safety, and a minimal environmental impact are equally important as performance. These features must be in the right balance to achieve the desired battery energy/power density and enhanced charge–discharge rate capability. From the discussion mentioned above, one of the best methods to improve the power performance of $\text{Li}_4\text{Ti}_5\text{O}_{12}$ is to increase its electronic conductivity using an effective hybrid surface coating. The hybrid nanocoating of the $\text{Li}_4\text{Ti}_5\text{O}_{12}$ anode has played an important role in improving its electrochemical performance.

Nevertheless, the synthesis usually involves low yields and complex procedures, high costs, and toxic precursors, which has limited explorations and applications. The development of controlled, large-scale, low-cost fabrication strategies for $\text{Li}_4\text{Ti}_5\text{O}_{12}$ anode nanomaterials with desirable performance is an important challenge in the fabrication of battery materials for wide-spread commercial application. Considering its promise in the design of a new generation of lithium-ion batteries, the graphene- $\text{Li}_4\text{Ti}_5\text{O}_{12}$ hybrid nanocomposite has potentially been shown to be a very promising material and might be used for high-rate power lithium-ion batteries due to its super electrochemical performance.

Acknowledgements

All financial support of the President's Award of University of Waterloo at Canada, the Postgraduate Scholarships from the Natural Sciences and Engineering Research Council of Canada (NSERC) and the Nano-fellowship from Waterloo Institute for Nanotechnology (WIN) at Canada has greatly been appreciated. P.V.R. thanks Canada Research Chairs program for a general support.

Notes and references

- 1 J.-M. Tarascon and M. Armand, *Nature*, 2001, **414**, 359.
- 2 P. G. Bruce, B. Scrosati and J. M. Tarascon, *Angew. Chem., Int. Ed.*, 2008, **47**, 2930.
- 3 T. Ohzuku, A. Ueda and N. Yamamoto, *J. Electrochem. Soc.*, 1995, **142**, 1431.
- 4 K. Zaghib, M. Simoneau, M. Armand and M. Gauthier, *J. Power Sources*, 1999, **81**, 300.
- 5 K. Nakahara, R. Nakajima, T. Matsushima and H. Majima, *J. Power Sources*, 2003, **117**, 131.
- 6 T.-F. Yi, L.-J. Jiang, J. Shu, C.-B. Yue, R.-S. Zhu and H.-B. Qiao, *J. Phys. Chem. Solids*, 2010, **71**, 1236.
- 7 K. Mukai, Y. Kato and H. Nakano, *J. Phys. Chem. C*, 2014, **118**, 2992.
- 8 W. Borghols, M. Wagemaker, U. Lafont, E. Kelder and F. Mulder, *J. Am. Chem. Soc.*, 2009, **131**, 17786.
- 9 P. Kubiak, A. Garcia, M. Womes, L. Aldon, J. Olivier-Fourcade, P.-E. Lippens and J.-C. Jumas, *J. Power Sources*, 2003, **119**, 626.
- 10 G. Wang, D. Bradhurst, S. Dou and H. Liu, *J. Power Sources*, 1999, **83**, 156.
- 11 L. Aldon, P. Kubiak, M. Womes, J. Jumas, J. Olivier-Fourcade, J. Tirado, J. Corredor and C. Pérez Vicente, *Chem. Mater.*, 2004, **16**, 5721.
- 12 J. Shu, *J. Solid State Electrochem.*, 2009, **13**, 1535.
- 13 N. Jovic, B. Antic, A. Kremenovic, A. Spasojevic-de Bire and V. Spasojevic, *Phys. Status Solidi A*, 2003, **198**, 18.
- 14 M. Wilkening, R. Amade, W. Iwaniak and P. Heijmans, *Phys. Chem. Chem. Phys.*, 2007, **9**, 1239.
- 15 E. M. Sorensen, S. J. Barry, H.-K. Jung, J. M. Rondinelli, J. T. Vaughey and K. R. Poeppelmeier, *Chem. Mater.*, 2006, **18**, 482.
- 16 G.-N. Zhu, Y.-G. Wang and Y.-Y. Xia, *Energy Environ. Sci.*, 2012, **5**, 6652.
- 17 S. Scharner, W. Weppner and P. Schmid-Beurmann, *J. Electrochem. Soc.*, 1999, **146**, 857.
- 18 W. Lu, I. Belharouak, J. Liu and K. Amine, *J. Electrochem. Soc.*, 2007, **154**, A114.
- 19 J. Ma, C. Wang and S. Wroblewski, *J. Power Sources*, 2007, **164**, 849.
- 20 N. Takami, K. Hoshina and H. Inagaki, *J. Electrochem. Soc.*, 2011, **158**, A725.
- 21 N. Takami, H. Inagaki, T. Kishi, Y. Harada, Y. Fujita and K. Hoshina, *J. Electrochem. Soc.*, 2009, **156**, A128.
- 22 J.-F. Colin, V. Godbole and P. Novák, *Electrochim. Commun.*, 2010, **12**, 804.
- 23 X. Yao, S. Xie, C. Chen, Q. Wang, J. Sun, Y. Li and S. Lu, *Electrochim. Acta*, 2005, **50**, 4076.
- 24 S.-I. Pyun, S.-W. Kim and H.-C. Shin, *J. Power Sources*, 1999, **81**, 248.
- 25 S. Bach, J. Pereira-Ramos and N. Baffier, *J. Power Sources*, 1999, **81**, 273.
- 26 P. P. Prosini, R. Mancini, L. Petrucci, V. Contini and P. Villano, *Solid State Ionics*, 2001, **144**, 185.
- 27 F. Ronci, P. Reale, B. Scrosati, S. Panero, V. Rossi Albertini, P. Perfetti, M. Di Michiel and J. Merino, *J. Phys. Chem. B*, 2002, **106**, 3082.
- 28 A. Jansen, A. Kahaian, K. Kepler, P. Nelson, K. Amine, D. Dees, D. Vissers and M. Thackeray, *J. Power Sources*, 1999, **81**, 902.
- 29 S. Panero, P. Reale, F. Ronci, V. R. Albertini and B. Scrosati, *Ionics*, 2000, **6**, 461.
- 30 P. Reale, S. Panero, B. Scrosati, J. Garche, M. Wohlfahrt-Mehrens and M. Wachtler, *J. Electrochem. Soc.*, 2004, **151**, A2138.
- 31 I. Leonidov, O. Leonidova, L. Perelyaeva, R. Samigullina, S. Kovayazina and M. Patrakeev, *Phys. Solid State*, 2003, **45**, 2183.
- 32 Z. Yang, D. Choi, S. Kerisit, K. M. Rosso, D. Wang, J. Zhang, G. Graff and J. Liu, *J. Power Sources*, 2009, **192**, 588.
- 33 S.-L. Chou, J.-Z. Wang, H.-K. Liu and S.-X. Dou, *J. Phys. Chem. C*, 2011, **115**, 16220.
- 34 K.-C. Hsiao, S.-C. Liao and J.-M. Chen, *Electrochim. Acta*, 2008, **53**, 7242.
- 35 Y.-B. He, B. Li, M. Liu, C. Zhang, W. Lv, C. Yang, J. Li, H. Du, B. Zhang and Q.-H. Yang, *Sci. Rep.*, 2012, **2**, 913.
- 36 H. Wu, Y. Huang, D. Jia, Z. Guo and M. Miao, *J. Nanopart. Res.*, 2012, **14**, 1.
- 37 X. Yao, S. Xie, H. Nian and C. Chen, *J. Alloys Compd.*, 2008, **465**, 375.
- 38 Y.-H. Jin, K.-M. Min, H.-W. Shim, S.-D. Seo, I.-S. Hwang, K.-S. Park and D.-W. Kim, *Nanoscale Res. Lett.*, 2012, **7**, 1.
- 39 M. Kalbáč, M. Zukalová and L. Kavan, *J. Solid State Electrochem.*, 2003, **8**, 2.
- 40 C. Jiang, Y. Zhou, I. Honma, T. Kudo and H. Zhou, *J. Power Sources*, 2007, **166**, 514.
- 41 D. Liu, C. Ouyang, J. Shu, J. Jiang, Z. Wang and L. Chen, *Phys. Status Solidi B*, 2006, **243**, 1835.
- 42 H. Ge, N. Li, D. Li, C. Dai and D. Wang, *J. Phys. Chem. C*, 2009, **113**, 6324.
- 43 C.-T. Hsieh and J.-Y. Lin, *J. Alloys Compd.*, 2010, **506**, 231.
- 44 S. Takai, M. Kamata, S. Fujine, K. Yoneda, K. Kanda and T. Esaka, *Solid State Ionics*, 1999, **123**, 165.
- 45 J. Gao, J. Ying, C. Jiang and C. Wan, *Ionics*, 2009, **15**, 597.
- 46 J. Chen, L. Yang, S. Fang and Y. Tang, *Electrochim. Acta*, 2010, **55**, 6596.
- 47 Y. Tang, L. Yang, S. Fang and Z. Qiu, *Electrochim. Acta*, 2009, **54**, 6244.
- 48 K. Naoi, S. Ishimoto, Y. Isobe and S. Aoyagi, *J. Power Sources*, 2010, **195**, 6250.
- 49 T.-F. Yi, J. Shu, C.-B. Yue, X.-D. Zhu, A.-N. Zhou, Y.-R. Zhu and R.-S. Zhu, *Mater. Res. Bull.*, 2010, **45**, 456.
- 50 C. Ouyang, Z. Zhong and M. Lei, *Electrochim. Commun.*, 2007, **9**, 1107.
- 51 Y. Hao, Q. Lai, Z. Xu, X. Liu and X. Ji, *Solid State Ionics*, 2005, **176**, 1201.
- 52 Z. Wen, S. Huang, X. Yang and B. Lin, *Solid State Ionics*, 2008, **179**, 1800.
- 53 J. Gao, C. Jiang, J. Ying and C. Wan, *J. Power Sources*, 2006, **155**, 364.

- 54 N. Zhu, W. Liu, M. Xue, Z. Xie, D. Zhao, M. Zhang, J. Chen and T. Cao, *Electrochim. Acta*, 2010, **55**, 5813.
- 55 M. Yoshio, R. J. Brodd and A. Kozawa, *Lithium-Ion Batteries*, Springer, 2009.
- 56 M. Winter and J. O. Besenhard, *Electrochim. Acta*, 1999, **45**, 31.
- 57 A. S. Aricò, P. Bruce, B. Scrosati, J.-M. Tarascon and W. Van Schalkwijk, *Nat. Mater.*, 2005, **4**, 366.
- 58 J. Garche, C. K. Dyer, P. T. Moseley, Z. Ogumi, D. A. Rand and B. Scrosati, *Encyclopedia of Electrochemical Power Sources*, Newnes, 2013.
- 59 M. M. Rahman, J.-Z. Wang, M. F. Hassan, S. Chou, D. Wexler and H.-K. Liu, *J. Power Sources*, 2010, **195**, 4297.
- 60 Y. Li, H. Zhao, Z. Tian, W. Qiu and X. Li, *J. Alloys Compd.*, 2008, **455**, 471.
- 61 J. Yang, J. Zhao, Y. Chen and Y. Li, *Ionics*, 2010, **16**, 425.
- 62 Y. Wang, H. Li, P. He, E. Hosono and H. Zhou, *Nanoscale*, 2010, **2**, 1294.
- 63 H. Li and H. Zhou, *Chem. Commun.*, 2012, **48**, 1201.
- 64 A. Y. Shenouda and K. Murali, *J. Power Sources*, 2008, **176**, 332.
- 65 W. Lu, I. Belharouak, J. Liu and K. Amine, *J. Power Sources*, 2007, **174**, 673.
- 66 P. Reale, A. Fornicola and B. Scrosati, *J. Power Sources*, 2009, **194**, 182.
- 67 A. Guerfi, P. Charest, K. Kinoshita, M. Perrier and K. Zaghib, *J. Power Sources*, 2004, **126**, 163.
- 68 S. Ji, J. Zhang, W. Wang, Y. Huang, Z. Feng, Z. Zhang and Z. Tang, *Mater. Chem. Phys.*, 2010, **123**, 510.
- 69 K. Kataoka, Y. Takahashi, N. Kijima, H. Hayakawa, J. Akimoto and K.-i. Ohshima, *Solid State Ionics*, 2009, **180**, 631.
- 70 X. Li, M. Qu, Y. Huai and Z. Yu, *Electrochim. Acta*, 2010, **55**, 2978.
- 71 X. Li, M. Qu and Z. Yu, *Solid State Ionics*, 2010, **181**, 635.
- 72 D. Capsoni, M. Bini, V. Massarotti, P. Mustarelli, G. Chiodelli, C. B. Azzoni, M. C. Mozzati, L. Linati and S. Ferrari, *Chem. Mater.*, 2008, **20**, 4291.
- 73 H. Ge, N. Li, D. Li, C. Dai and D. Wang, *Electrochim. Commun.*, 2008, **10**, 719.
- 74 G. Wang, J. Xu, M. Wen, R. Cai, R. Ran and Z. Shao, *Solid State Ionics*, 2008, **179**, 946.
- 75 G. Liu, L. Wen, G. Liu, Q. Wu, H. Luo, B. Ma and Y. Tian, *J. Alloys Compd.*, 2011, **509**, 6427.
- 76 X. Sun, M. Hegde, J. Wang, Y. Zhang, J. Liao, P. V. Radovanovic and B. Cui, *ECS Trans.*, 2014, **58**, 79.
- 77 C.-H. Hong, A. Noviyanto, J. H. Ryu, J. Kim and D.-H. Yoon, *Ceram. Int.*, 2012, **38**, 301.
- 78 J. W. Shin, C. H. Hong and D. H. Yoon, *J. Am. Ceram. Soc.*, 2012, **95**, 1894.
- 79 T. Yuan, R. Cai, P. Gu and Z. Shao, *J. Power Sources*, 2010, **195**, 2883.
- 80 J. Li, Y.-L. Jin, X.-G. Zhang and H. Yang, *Solid State Ionics*, 2007, **178**, 1590.
- 81 Y. Bai, F. Wang, F. Wu, C. Wu and L.-Y. Bao, *Electrochim. Acta*, 2008, **54**, 322.
- 82 K. Teshima, H. Inagaki, S. Tanaka, K. Yubuta, M. Hozumi, K. Kohama, T. Shishido and S. Oishi, *Cryst. Growth Des.*, 2011, **11**, 4401.
- 83 S. C. Lee, S. M. Lee, J. W. Lee, J. B. Lee, S. M. Lee, S. S. Han, H. C. Lee and H. J. Kim, *J. Phys. Chem. C*, 2009, **113**, 18420.
- 84 Y. Tang, L. Yang, Z. Qiu and J. S. Huang, *Electrochim. Commun.*, 2008, **10**, 1513.
- 85 Y. Tang, L. Yang, Z. Qiu and J. Huang, *J. Mater. Chem.*, 2009, **19**, 5980.
- 86 L. Shen, C. Yuan, H. Luo, X. Zhang, K. Xu and Y. Xia, *J. Mater. Chem.*, 2010, **20**, 6998.
- 87 C. Lai, Y. Dou, X. Li and X. Gao, *J. Power Sources*, 2010, **195**, 3676.
- 88 J. Chen, L. Yang, S. Fang, S.-I. Hirano and K. Tachibana, *J. Power Sources*, 2012, **200**, 59.
- 89 J. Liu, X. Li, J. Yang, D. Geng, Y. Li, D. Wang, R. Li, X. Sun, M. Cai and M. W. Verbrugge, *Electrochim. Acta*, 2012, **63**, 100.
- 90 X. C. Sun, M. Hegde, Y. Zhang, M. He, L. Gu, Y. Wang, J. Shu, P. V. Radovanovic and B. Cui, *Int. J. Electrochem. Sci.*, 2014, **9**, 1583.
- 91 A. Laumann, M. Bremholm, P. Hald, M. Holzapfel, K. T. Fehr and B. B. Iversen, *J. Electrochem. Soc.*, 2011, **159**, A166.
- 92 L. Shen, C. Yuan, H. Luo, X. Zhang, K. Xu and F. Zhang, *J. Mater. Chem.*, 2011, **21**, 761.
- 93 S.-H. Yu, A. Pucci, T. Herntrich, M.-G. Willinger, S.-H. Baek, Y.-E. Sung and N. Pinna, *J. Mater. Chem.*, 2011, **21**, 806.
- 94 C.-M. Shen, X.-G. Zhang, Y.-K. Zhou and H.-L. Li, *Mater. Chem. Phys.*, 2003, **78**, 437.
- 95 M.-H. Oh, H.-J. Kim, Y. J. Kim, K. J. Kim and S.-G. Park, *ECS Trans.*, 2007, **3**, 101.
- 96 N. Alias, M. Kufian, L. Teo, S. Majid and A. Arof, *J. Alloys Compd.*, 2009, **486**, 645.
- 97 R. B. Khomane, A. Prakash, K. Ramesha and M. Sathiya, *Mater. Res. Bull.*, 2011, **46**, 1139.
- 98 M. Venkateswarlu, C. Chen, J. Do, C. Lin, T.-C. Chou and B. Hwang, *J. Power Sources*, 2005, **146**, 204.
- 99 N. Zhang, Z. Liu, T. Yang, C. Liao, Z. Wang and K. Sun, *Electrochim. Commun.*, 2011, **13**, 654.
- 100 Y.-J. Hao, Q.-Y. Lai, J.-Z. Lu, D.-Q. Liu and X.-Y. Ji, *J. Alloys Compd.*, 2007, **439**, 330.
- 101 M. Mohammadi and D. Fray, *J. Sol-Gel Sci. Technol.*, 2010, **55**, 19.
- 102 Y. H. Rho and K. Kanamura, *J. Solid State Chem.*, 2004, **177**, 2094.
- 103 G. Yan, H. Fang, H. Zhao, G. Li, Y. Yang and L. Li, *J. Alloys Compd.*, 2009, **470**, 544.
- 104 Y. Hao, Q.-Y. Lai, D. Liu, Z.-U. Xu and X. Ji, *Mater. Chem. Phys.*, 2005, **94**, 382.
- 105 Y.-J. Hao, Q.-Y. Lai, J.-Z. Lu, H.-L. Wang, Y.-D. Chen and X.-Y. Ji, *J. Power Sources*, 2006, **158**, 1358.
- 106 A. Mukasyan and P. Dinka, *Int. J. Self-Propag. High-Temp. Synth.*, 2007, **16**, 23.
- 107 K. C. Patil, S. Aruna and T. Mimani, *Curr. Opin. Solid State Mater. Sci.*, 2002, **6**, 507.

- 108 S. T. Aruna and A. S. Mukasyan, *Curr. Opin. Solid State Mater. Sci.*, 2008, **12**, 44.
- 109 A. Prakash, P. Manikandan, K. Ramesha, M. Sathiya, J. Tarascon and A. Shukla, *Chem. Mater.*, 2010, **22**, 2857.
- 110 M. Raja, S. Mahanty, M. Kundu and R. N. Basu, *J. Alloys Compd.*, 2009, **468**, 258.
- 111 T. Yuan, R. Cai, K. Wang, R. Ran, S. Liu and Z. Shao, *Ceram. Int.*, 2009, **35**, 1757.
- 112 G. L. Messing, S. C. Zhang and G. V. Jayanthi, *J. Am. Ceram. Soc.*, 1993, **76**, 2707.
- 113 D. S. Jung, S. B. Park and Y. C. Kang, *Korean J. Chem. Eng.*, 2010, **27**, 1621.
- 114 S. H. Ju and Y. C. Kang, *J. Phys. Chem. Solids*, 2009, **70**, 40.
- 115 S. H. Ju and Y. C. Kang, *J. Power Sources*, 2009, **189**, 185.
- 116 S. H. Ju and Y. C. Kang, *J. Alloys Compd.*, 2010, **506**, 913.
- 117 S. Yin, L. Song, X. Wang, M. Zhang, K. Zhang and Y. Zhang, *Electrochim. Acta*, 2009, **54**, 5629.
- 118 T. Yuan, K. Wang, R. Cai, R. Ran and Z. Shao, *J. Alloys Compd.*, 2009, **477**, 665.
- 119 D. Kim, Y. Ahn and J. Kim, *Electrochim. Commun.*, 2005, **7**, 1340.
- 120 S. S. Lee, K.-T. Byun, J. P. Park, S. K. Kim, H.-Y. Kwak and I.-W. Shim, *Dalton Trans.*, 2007, 4182.
- 121 T. Doi, Y. Iriyama, T. Abe and Z. Ogumi, *Chem. Mater.*, 2005, **17**, 1580.
- 122 F. Ernst, H. Kammler, A. Roessler, S. Pratsinis, W. Stark, J. Ufheil and P. Novák, *Mater. Chem. Phys.*, 2007, **101**, 372.
- 123 J. Wolfenstine and J. Allen, *J. Power Sources*, 2008, **180**, 582.
- 124 X. L. Zhang, G. R. Hu and Z. D. Peng, *J. Cent. South Univ.*, 2013, **20**, 1151.
- 125 T.-F. Yi, H. Liu, Y.-R. Zhu, L.-J. Jiang, Y. Xie and R.-S. Zhu, *J. Power Sources*, 2012, **215**, 258.
- 126 Z. Yu, X. Zhang, G. Yang, J. Liu, J. Wang, R. Wang and J. Zhang, *Electrochim. Acta*, 2011, **56**, 8611.
- 127 L. Xing, *Chin. J. Inorg. Chem.*, 2010, **2**, 233.
- 128 T.-F. Yi, Y. Xie, Q. Wu, H. Liu, L. Jiang, M. Ye and R. Zhu, *J. Power Sources*, 2012, **214**, 220.
- 129 B. Zhang, Z.-D. Huang, S. W. Oh and J.-K. Kim, *J. Power Sources*, 2011, **196**, 10692.
- 130 C. Chen, J. Vaughey, A. Jansen, D. Dees, A. Kahaian, T. Goacher and M. Thackeray, *J. Electrochem. Soc.*, 2001, **148**, A102.
- 131 R. Cai, S. Jiang, X. Yu, B. Zhao, H. Wang and Z. Shao, *J. Mater. Chem.*, 2012, **22**, 8013.
- 132 D. Wu and Y. Cheng, *Ionics*, 2013, **19**, 395.
- 133 S. Huang, Z. Wen, Z. Gu and X. Zhu, *Electrochim. Acta*, 2005, **50**, 4057.
- 134 S. Huang, Z. Wen, X. Zhu and Z. Lin, *J. Power Sources*, 2007, **165**, 408.
- 135 J.-Y. Lin, C.-C. Hsu, H.-P. Ho and S.-H. Wu, *Electrochim. Acta*, 2013, **87**, 126.
- 136 Z. Wang, G. Chen, J. Xu, Z. Lv and W. Yang, *J. Phys. Chem. Solids*, 2011, **72**, 773.
- 137 Y.-J. Hao, Q.-Y. Lai, J.-Z. Lu and X.-Y. Ji, *Ionics*, 2007, **13**, 369.
- 138 W. Long, X. Wang, S. Yang, H. Shu, Q. Wu, Y. Bai and L. Bai, *Mater. Chem. Phys.*, 2011, **131**, 431.
- 139 A. Robertson, L. Trevino, H. Tukamoto and J. Irvine, *J. Power Sources*, 1999, **81**, 352.
- 140 J. Gao, C. Jiang and C. Wan, *J. Electrochem. Soc.*, 2010, **157**, K39.
- 141 Y.-J. Bai, C. Gong, Y.-X. Qi, N. Lun and J. Feng, *J. Mater. Chem.*, 2012, **22**, 19054.
- 142 Y.-J. Bai, C. Gong, N. Lun and Y.-X. Qi, *J. Mater. Chem. A*, 2013, **1**, 89.
- 143 C. Qiu, Z. Yuan, L. Liu, N. Ye and J. Liu, *J. Solid State Electrochem.*, 2013, **17**, 841.
- 144 K. Abhilash, P. C. Selvin, B. Nalini, P. Nithyadharseni and B. Pillai, *Ceram. Int.*, 2013, **39**, 947.
- 145 X. Li, M. Qu and Z. Yu, *J. Alloys Compd.*, 2009, **487**, L12.
- 146 Y.-R. Jhan and J.-G. Duh, *Electrochim. Acta*, 2012, **63**, 9.
- 147 V. Nithya, R. Kalai Selvan, K. Vediappan, S. Sharmila and C. W. Lee, *Appl. Surf. Sci.*, 2012, **261**, 515.
- 148 T.-F. Yi, J. Shu, Y.-R. Zhu, X.-D. Zhu, C.-B. Yue, A.-N. Zhou and R.-S. Zhu, *Electrochim. Acta*, 2009, **54**, 7464.
- 149 Z. Zhong, *Electrochim. Solid-State Lett.*, 2007, **10**, A267.
- 150 B. Tian, H. Xiang, L. Zhang, Z. Li and H. Wang, *Electrochim. Acta*, 2010, **55**, 5453.
- 151 B. Tian, H. Xiang, L. Zhang and H. Wang, *J. Solid State Electrochem.*, 2012, **16**, 205.
- 152 T.-F. Yi, Y. Xie, J. Shu, Z. Wang, C.-B. Yue, R.-S. Zhu and H.-B. Qiao, *J. Electrochim. Soc.*, 2011, **158**, A266.
- 153 W. Wang, H. Wang, S. Wang, Y. Hu, Q. Tian and S. Jiao, *J. Power Sources*, 2013, **228**, 244.
- 154 R. Cai, T. Yuan, R. Ran, X. Liu and Z. Shao, *Int. J. Energy Res.*, 2011, **35**, 68.
- 155 J.-P. Zhu, J.-J. Zhao, H.-W. Yang and G. Yang, *Adv. Sci. Lett.*, 2011, **4**, 484.
- 156 B. Zhang, H. Du, B. Li and F. Kang, *Electrochim. Solid-State Lett.*, 2010, **13**, A36.
- 157 S. Huang, Z. Wen, B. Lin, J. Han and X. Xu, *J. Alloys Compd.*, 2008, **457**, 400.
- 158 Q. Zhang, C. Zhang, B. Li, S. Kang, X. Li and Y. Wang, *Electrochim. Acta*, 2013, **98**, 146.
- 159 H. Zhao, Y. Li, Z. Zhu, J. Lin, Z. Tian and R. Wang, *Electrochim. Acta*, 2008, **53**, 7079.
- 160 G. Du, N. Sharma, V. K. Peterson, J. A. Kimpton, D. Jia and Z. Guo, *Adv. Funct. Mater.*, 2011, **21**, 3990.
- 161 Y. Qi, Y. Huang, D. Jia, S.-J. Bao and Z. Guo, *Electrochim. Acta*, 2009, **54**, 4772.
- 162 Y. Huang, Y. Qi, D. Jia, X. Wang, Z. Guo and W. I. Cho, *J. Solid State Electrochem.*, 2012, **16**, 2011.
- 163 Y. Ma, B. Ding, G. Ji and J. Y. Lee, *ACS Nano*, 2013, **7**, 10870.
- 164 S. Huang, Z. Wen, X. Zhu and X. Yang, *J. Electrochim. Soc.*, 2005, **152**, A1301.
- 165 Y.-Y. Wang, Y.-J. Hao, Q.-Y. Lai, J.-Z. Lu, Y.-D. Chen and X.-Y. Ji, *Ionics*, 2008, **14**, 85.
- 166 M. Rahman, J.-Z. Wang, M. F. Hassan, S. Chou, D. Wexler and H.-K. Liu, *J. Power Sources*, 2010, **195**, 4297.
- 167 J. Lim, E. Choi, V. Mathew, D. Kim, D. Ahn, J. Gim, S.-H. Kang and J. Kim, *J. Electrochim. Soc.*, 2011, **158**, A275.
- 168 Y. Wang, H. Liu, K. Wang, H. Eiji, Y. Wang and H. Zhou, *J. Mater. Chem.*, 2009, **19**, 6789.

- 169 A. Jaiswal, C. Horne, O. Chang, W. Zhang, W. Kong, E. Wang, T. Chern and M. Doeff, *J. Electrochem. Soc.*, 2009, **156**, A1041.
- 170 J. Kim and J. Cho, *Electrochem. Solid-State Lett.*, 2007, **10**, A81.
- 171 C. Jiang, M. Ichihara, I. Honma and H. Zhou, *Electrochim. Acta*, 2007, **52**, 6470.
- 172 L. Yu, H. B. Wu and X. W. D. Lou, *Adv. Mater.*, 2013, **25**, 2296.
- 173 X. Lu, L. Zhao, X. He, R. Xiao, L. Gu, Y. S. Hu, H. Li, Z. Wang, X. Duan and L. Chen, *Adv. Mater.*, 2012, **24**, 3233.
- 174 K.-S. Park, A. Benayad, D.-J. Kang and S.-G. Doo, *J. Am. Chem. Soc.*, 2008, **130**, 14930.
- 175 M. R. Jo, Y. S. Jung and Y.-M. Kang, *Nanoscale*, 2012, **4**, 6870.
- 176 L. Wang, Q. Xiao, Z. Li, G. Lei, P. Zhang and L. Wu, *J. Solid State Electrochem.*, 2012, **16**, 3307.
- 177 Z. Hong, T. Lan, F. Xiao, H. Zhang and M. Wei, *Funct. Mater. Lett.*, 2011, **4**, 389.
- 178 N. He, B. Wang and J. Huang, *J. Solid State Electrochem.*, 2010, **14**, 1241.
- 179 D. Shao, J. He, Y. Luo, W. Liu, X. Yu and Y. Fang, *J. Solid State Electrochem.*, 2012, **16**, 2047.
- 180 Y.-S. Lin and J.-G. Duh, *J. Power Sources*, 2011, **196**, 10698.
- 181 H.-G. Jung, S.-T. Myung, C. S. Yoon, S.-B. Son, K. H. Oh, K. Amine, B. Scrosati and Y.-K. Sun, *Energy Environ. Sci.*, 2011, **4**, 1345.
- 182 L. Cheng, J. Yan, G.-N. Zhu, J.-Y. Luo, C.-X. Wang and Y.-Y. Xia, *J. Mater. Chem.*, 2010, **20**, 595.
- 183 B. Li, C. Han, Y.-B. He, C. Yang, H. Du, Q.-H. Yang and F. Kang, *Energy Environ. Sci.*, 2012, **5**, 9595.
- 184 J. Gao, J. Ying, C. Jiang and C. Wan, *J. Power Sources*, 2007, **166**, 255.
- 185 G. J. Wang, J. Gao, L. J. Fu, N. H. Zhao, Y. P. Wu and T. Takamura, *J. Power Sources*, 2007, **174**, 1109.
- 186 L. Cheng, X.-L. Li, H.-J. Liu, H.-M. Xiong, P.-W. Zhang and Y.-Y. Xia, *J. Electrochem. Soc.*, 2007, **154**, A692.
- 187 G.-N. Zhu, C.-X. Wang and Y.-Y. Xia, *J. Electrochem. Soc.*, 2011, **158**, A102.
- 188 H. Ming, J. Ming, X. Li, Q. Zhou, H. Wang, L. Jin, Y. Fu, J. Adkins and J. Zheng, *Electrochim. Acta*, 2014, **116**, 224.
- 189 H. Li, L. Shen, K. Yin, J. Ji, J. Wang, X. Wang and X. Zhang, *J. Mater. Chem. A*, 2013, **1**, 7270.
- 190 L. Yang and L. Gao, *J. Alloys Compd.*, 2009, **485**, 93.
- 191 Z. Zhu, F. Cheng and J. Chen, *J. Mater. Chem. A*, 2013, **1**, 9484.
- 192 L. Zhao, Y. S. Hu, H. Li, Z. Wang and L. Chen, *Adv. Mater.*, 2011, **23**, 1385.
- 193 M. Inagaki, *Carbon*, 2012, **50**, 3247.
- 194 M. Gaberscek and J. Jamnik, *Solid State Ionics*, 2006, **177**, 2647.
- 195 R. Dominko, M. Bele, M. Gaberscek, M. Remskar, D. Hanzel, S. Pejovnik and J. Jamnik, *J. Electrochem. Soc.*, 2005, **152**, A607.
- 196 X. C. Sun, M. Hegde, J. Wang, Y. Zhang, J. Liao, P. V. Radovanovic and B. Cui, *ECS Trans.*, 2014, **58**, 79.
- 197 J. Wang, X.-M. Liu, H. Yang and X.-D. Shen, *J. Alloys Compd.*, 2011, **509**, 712.
- 198 H. Luo, L. Shen, K. Rui, H. Li and X. Zhang, *J. Alloys Compd.*, 2013, **572**, 37.
- 199 H.-G. Jung, J. Kim, B. Scrosati and Y.-K. Sun, *J. Power Sources*, 2011, **196**, 7763.
- 200 Z. Lin, X. Hu, Y. Huai, L. Liu, Z. Deng and J. Suo, *Solid State Ionics*, 2010, **181**, 412.
- 201 H. Liu, Y. Feng, K. Wang and J. Xie, *J. Phys. Chem. Solids*, 2008, **69**, 2037.
- 202 X. Guo, H. F. Xiang, T. P. Zhou, X. K. Ju and Y. C. Wu, *Electrochim. Acta*, 2014, **130**, 470.
- 203 A. K. Geim and K. S. Novoselov, *Nat. Mater.*, 2007, **6**, 183.
- 204 A. K. Geim, *Science*, 2009, **324**, 1530.
- 205 L. Shen, C. Yuan, H. Luo, X. Zhang, S. Yang and X. Lu, *Nanoscale*, 2011, **3**, 572.
- 206 Y. Shi, L. Wen, F. Li and H.-M. Cheng, *J. Power Sources*, 2011, **196**, 8610.
- 207 Y. Oh, S. Nam, S. Wi, J. Kang, T. Hwang, S. Lee, H. H. Park, J. Cabana, C. Kim and B. Park, *J. Mater. Chem. A*, 2014, **2**, 2023.
- 208 Q. Zhang, W. Peng, Z. Wang, X. Li, X. Xiong, H. Guo, Z. Wang and F. Wu, *Ionics*, 2013, **19**, 717.
- 209 A. K. Rai, J. Gim, S.-W. Kang, V. Mathew, L. T. Anh, J. Kang, J. Song, B. J. Paul and J. Kim, *Mater. Chem. Phys.*, 2012, **136**, 1044.
- 210 S. Y. Han, I. Y. Kim, K. Y. Jo and S.-J. Hwang, *J. Phys. Chem. C*, 2012, **116**, 7269.
- 211 S. Pang, Y. Zhao, C. Zhang, Q. Zhang, L. Gu, X. Zhou, G. Li and G. Cui, *Scr. Mater.*, 2013, **69**, 171.
- 212 H. Xiang, B. Tian, P. Lian, Z. Li and H. Wang, *J. Alloys Compd.*, 2011, **509**, 7205.
- 213 S. G. Ri, L. Zhan, Y. Wang, L. Zhou, J. Hu and H. Liu, *Electrochim. Acta*, 2013, **109**, 389.
- 214 H. Ni, W.-L. Song and L.-Z. Fan, *Electrochem. Commun.*, 2014, **40**, 1.
- 215 X. Guo, H. F. Xiang, T. P. Zhou, W. H. Li, X. W. Wang, J. X. Zhou and Y. Yu, *Electrochim. Acta*, 2013, **109**, 33.
- 216 X. Wang, L. Shen, H. Li, J. Wang, H. Dou and X. Zhang, *Electrochim. Acta*, 2014, **129**, 283.
- 217 C. Sandhya, B. John and C. Gouri, *Ionics*, 2014, **20**, 601.
- 218 E. Ferg, R. Gummow, A. De Kock and M. Thackeray, *J. Electrochem. Soc.*, 1994, **141**, L147.
- 219 B. Scrosati and J. Garche, *J. Power Sources*, 2010, **195**, 2419.
- 220 W. Lu, J. Liu, Y. K. Sun and K. Amine, *J. Power Sources*, 2007, **167**, 212.
- 221 C. M. Ionica-Bousquet, D. Muñoz-Rojas, W. J. Casteel, R. M. Pearlstein, G. GirishKumar, G. P. Pez and M. R. Palacín, *J. Power Sources*, 2010, **195**, 1479.
- 222 I. Belharouak, Y.-K. Sun, W. Lu and K. Amine, *J. Electrochem. Soc.*, 2007, **154**, A1083.
- 223 I. Belharouak, G. M. Koenig, T. Tan, H. Yumoto, N. Ota and K. Amine, *J. Electrochem. Soc.*, 2012, **159**, A1165.
- 224 K. Amine, I. Belharouak, Z. Chen, T. Tran, H. Yumoto, N. Ota, S. T. Myung and Y. K. Sun, *Adv. Mater.*, 2010, **22**, 3052.
- 225 X. Hu, Z. Deng, J. Suo and Z. Pan, *J. Power Sources*, 2009, **187**, 635.

- 226 S. Panero, D. Satolli, M. Salomon and B. Scrosati, *Electrochem. Commun.*, 2000, **2**, 810.
- 227 V. Etacheri, R. Marom, R. Elazari, G. Salitra and D. Aurbach, *Energy Environ. Sci.*, 2011, **4**, 3243.
- 228 S. K. Martha, O. Haik, V. Borgel, E. Zinigrad, I. Exnar, T. Drezen, J. H. Miners and D. Aurbach, *J. Electrochem. Soc.*, 2011, **158**, A790.
- 229 V. Borgel, G. Gershinsky, T. Hu, M. G. Theivanayagam and D. Aurbach, *J. Electrochem. Soc.*, 2013, **160**, A650.
- 230 H. Wu, I. Belharouak, H. Deng, A. Abouimrane, Y.-K. Sun and K. Amine, *J. Electrochem. Soc.*, 2009, **156**, A1047.
- 231 S. Li, C. Chen and J. Dahn, *J. Electrochem. Soc.*, 2013, **160**, A2166.
- 232 I. Belharouak, G. M. Koenig Jr and K. Amine, *J. Power Sources*, 2011, **196**, 10344.
- 233 A. Du Pasquier, C. C. Huang and T. Spitler, *J. Power Sources*, 2009, **186**, 508.
- 234 N. M. Hagh and G. G. Amatucci, *J. Power Sources*, 2010, **195**, 5005.
- 235 S. Li, C. Chen, X. Xia and J. Dahn, *J. Electrochem. Soc.*, 2013, **160**, A1524.
- 236 L. Q. Sun, R. H. Cui, A. F. Jalbout, M. J. Li, X. M. Pan, R. S. Wang and H. M. Xie, *J. Power Sources*, 2009, **189**, 522.
- 237 K. Zaghib, M. Dontigny, A. Guerfi, P. Charest, I. Rodrigues, A. Mauger and C. Julien, *J. Power Sources*, 2011, **196**, 3949.
- 238 K. Zaghib, M. Dontigny, A. Guerfi, J. Trottier, J. Hamel-Paquet, V. Gariepy, K. Galoutov, P. Hovington, A. Mauger, H. Grout and C. M. Julien, *J. Power Sources*, 2012, **216**, 192.
- 239 K. Ariyoshi, S. Yamamoto and T. Ohzuku, *J. Power Sources*, 2003, **119–121**, 959.
- 240 H. F. Xiang, Q. Y. Jin, R. Wang, C. H. Chen and X. W. Ge, *J. Power Sources*, 2008, **179**, 351.
- 241 M. Reddy, G. Subba Rao and B. Chowdari, *Chem. Rev.*, 2013, **113**, 5364.
- 242 W. W. Lee and J.-M. Lee, *J. Mater. Chem. A*, 2014, **2**, 1589.